Holocene phototrophic community and anoxia dynamics in meromictic Lake Jaczno (NE Poland) using high-resolution hyperspectral imaging and HPLC data.

Stamatina Makri[1], Andrea Lami[2], Luyao Tu[1], Wojciech Tylmann[3], Hendrik Vogel[4,] Martin Grosjean[1]

[1]Institute of Geography & Oeschger Centre for Climate Change Research, University of Bern, Hallerstrasse 12, 3012 Bern, Switzerland

[2]ISE-CNR Institute of Ecosystem Study, 50 Largo Tonolli, 28922 Verbania Pallanza, Italy

[3]Faculty of Oceanography and Geography, University of Gdansk, Bazynskiego 4, PL-80952 Gdansk, Poland

[4]Institute of Geological Sciences & Oeschger Centre for Climate Change Research, University of Bern, 3012, Bern, Switzerland

Correspondence to: Stamatina Makri (stamatina.makri@giub.unibe.ch)

Abstract. Global spread of hypoxia and less frequent mixing in lakes is a growing major environmental concern. Climate change and human impact are expected to increasingly deteriorate aquatic ecosystems. The study of processes and drivers of such changes in the past provides a great asset for prevention and remediation in the future. We used a multi-proxy approach combining high-resolution bulk pigment data measured by Hyperspectral Imaging (HSI), with lower resolution specific chlorophylls and carotenoids measured by HPLC to examine Holocene trophic state changes
and anoxia evolution in meromictic Lake Jaczno, NE Poland. A redundancy analysis RDA including pollen-inferred vegetation cover, temperature and human impacts provides insight into specific conditions and drivers of changing trophic and redox states in the lake. Anoxic and sulfidic conditions established in Lake Jaczno after initial basin infilling 9500 years ago. Until 6700 cal BP, lake trophy was relatively low, water turbidity was high, and green sulfur bacteria (GSB) were abundant within the phototrophic community, suggesting a deep oxic–anoxic boundary and weak stratification. The period between 6700–500 cal BP is characterized by constantly increasing lake production and a gradual shift from GSB to purple sulfur bacteria (PSB), suggesting a shallower oxic–anoxic boundary and pronounced stratification. Yet, the presence of spheroidene and speroidenone in the sediments indicates intermittent anoxia. After 500 cal BP, increasing human impact, deforestation and intensive agriculture promoted lake eutrophication, with a shift to PSB dominance and establishment of permanent anoxia and meromixis. Our study unambiguously documents the legacy of human impact on processes determining eutrophication and anoxia.

Keywords: Paleolimnology, Anoxia, Meromixis, Varved sediments, North–East Europe, Holocene, Sedimentary pigments, Human impact

1. Introduction

Eutrophication and subsequent oxygen depletion have become primary water quality issues for most freshwater and coastal marine ecosystems globally (Schindler, 2006; Jenny et al., 2016a). Rising mean global temperature

can potentially worsen lake anoxia by enhancing water stratification and algal blooms (Adrian et al., 2009; Woolway and Merchant, 2019). Higher lake trophy and reducing conditions in anoxic bottom waters can have diverse and profound negative effects on lake ecosystems, such as toxic algal blooms, fish kills, biodiversity loss (Smol, 2010; Battarbee and Bennion, 2012; Makri et al., 2019), and nutrient recycling into the water column from the sediment through redox processes (Gächter, 1987; Tu et al., 2019). Hence, the global spread of hypoxia grows into a major environmental concern (Diaz and Rosenberg, 2008).

Temporal and spatial extents of hypoxia/anoxia are influenced by both biological (aquatic production, organic matter decomposition) and physical (water stratification and lake mixing) factors (Smith and Schindler, 2009; Friedrich et al., 2014; Jenny et al., 2016b). Environmental and climatic effects such as temperature, seasonality and extreme events, catchment vegetation, land use, human impact and nutrient input affect lake production and oxygen supply in the bottom waters.

Observational data of anoxia and aquatic production cover usually only very short periods, which restricts the understanding of relevant processes and the knowledge of pre-disturbance conditions. This is most relevant for lake management or restoration. Although recent anoxia and eutrophication have been very well studied and understood (Naeher et al., 2013; Friedrich et al., 2014; Jenny et al., 2016a), less is known about the onset, cessation and specific conditions of these changes in the past due to the lack of effective and easily measurable proxies (Friedrich et al., 2014; Makri et al., 2020). More specifically, to assess lake trophy and/or bottom water oxygenation, proxies such as sedimentary pigments (Lami et al., 2000; Leavitt and Hodgson, 2001; Guilizzoni and Lami, 2002), lipid biomarkers (Naeher et al., 2012), diatom (Bennion and Simpson, 2011) and chironomid records (Little et al., 2000), stable isotopes (Pearson and Coplen, 1978), and redox sensitive elements such as Fe, Mn, Mo, V, and U (Naeher et al., 2013; Wirth et al., 2013; Costa et al., 2015), have been extensively used so far. Nonetheless, on long-term Holocene time-scales, most of these proxy records are typically established at a centennial resolution at best.

Laminated lake sediments are valuable archives of natural and anthropogenic impacts, providing long-term records via various biogeochemical proxies. Sedimentary photosynthetic pigment records can be effectively used to infer both changes in algal composition and lake oxygen conditions (Guilizzoni et al., 1983; Leavitt, 1993; Lami et al., 2000). Chlorophylls, together with their derivatives, and various carotenoids specific to particular groups of algae can be used to reconstruct overall primary production and the composition of past photosynthetic communities (Leavitt and Hodgson, 2001). Pigments such as okenone and isorenieratene, which are specific to phototrophic sulfur bacteria that live in the anoxic sulfidic zones, are regarded as very good indicators of anoxia (Züllig, 1989; Guilizzoni and Lami, 2002). HPLC-inferred pigments have a coarser temporal resolution due to laborious sample preparation and time-consuming HPLC measurements. Scanning Hyperspectral Imaging (HSI), a novel non-destructive method to quantitatively infer the abundance of algal (TChl: chlorophyll *a* and *b*, and their derivatives) and bacterial pigments (Bphe: bacteriopheophytins *a* and *b*), offers insight into past trophic and oxygen conditions at unprecedented μm-scale (sub-seasonal) resolution (Butz et al., 2015; Makri et al., 2020), but with lower speciation sensitivity.

78   In this study, we use the varved sediment record of Lake Jaczno (NE Poland) to explore the specific conditions
79   and mechanisms of trophic and oxygen state changes in the Holocene, under changing climatic and environmental
80   conditions. Our research has been guided by the following questions: i) Which conditions drove algae dynamics
81   and oxygen state changes in the Holocene before any significant human intervention? ii) How did climate,
82   catchment vegetation and erosional input affected the phototrophic community in the lake and iii) How does the
83   current trophic state and mixing regime of the lake compare with the past? For this, we combined a high-resolution
84   HSI-inferred record of TChl and Bphe, X-ray fluorescence (XRF) elemental data, and a low-resolution pigment
85   record using HPLC analysis with high compound specificity, which cannot be achieved by the HSI record. Our
86   dataset was compared with vegetation and temperature reconstruction data to investigate the environmental
87   conditions at times of aquatic primary production and bottom water oxygenation changes. Lake Jaczno provides
88   ideal conditions to answer these questions. It contains an entirely varved Holocene sediment record, which has so
89   far only been analyzed for the last 1700 years for productivity, anoxia (Butz et al., 2016, 2017) and historical land
90   use (Poraj-Górska et al., 2017). Pollen records have revealed that human pressure was low until the 17th century,
91   when landscapes opened and agriculture intensified (Marcisz et al., 2020). Therefore, this site provides a unique
92   opportunity for a long-term Holocene assessment of the natural causes and dynamics of meromixis and hypoxia
93   with limited anthropogenic impact until historic times.

94   **2.   Study site**

95   Lake Jaczno (54°16'25.5" N 22°52'15.9" E, 163 m a.s.l, Fig. 1a) is a small, 26 m deep, exoreic, kettle-hole lake
96   formed sometime after the Weichselian deglaciation ca. 15 ka BP in the Suwałki Lakeland in NE Poland
97   (Krzywicki, 2002). Lake Jaczno has a total surface area of 0.41 km^2 separated in five distinct basins with narrow
98   sills. It is fed by three permanent inflows (N and W) and one outflow in the south (Fig. 1b). Jaczno is classified as
99   dimictic and mesotrophic (Tylmann et al., 2013), with incomplete mixing or possibly even meromixis during some
100   years (Butz et al., 2016). Butz at al. (2017) found that anoxic, and even meromictic conditions, established naturally
101   for most of the past 1700 years. Meromixis was interrupted repeatedly following sediment slumping or flood
102   events.

103   Microscopic and geochemical analyses in the sediments of Lake Jaczno have revealed seasonal layers (calcareous
104   biogenic varves) with a complex succession of diatoms and calcite, detrital siliciclastic material (quartz, clays),
105   organic fragments, and finally amorphous organic matter (Tylmann et al., 2013; Butz et al., 2016; Poraj-Górska et
106   al., 2017). The lake is surrounded by steep slopes and gullies with ephemeral or perennial water flow, transporting
107   detrital material to the lake (Fig. 1c).
108
109   The catchment area (ca. 9 km^2) is covered by glacial tills, sands and fluvioglacial deposits. Modern soils are
110   classified as cambisols and podsols in the northern part and ferralic cambisols in the southern part of the catchment.
111   Agricultural lands dominate in the central and northern parts and forests in the southern parts (Fig. 1c). The lake
112   is surrounded by peatlands and forests dominated by birch, alder and spruce (Weisbrodt et al., 2017). The climate
113   of the region is continental with a mean annual temperature of 6.8°C and a mean annual precipitation of 600 mm
114   (IMGW-PIB, 2017). The lakes in the area typically remain ice covered from December to March (Amann et al.,
115   2014).

116 Archeological investigations in the Suwałki region indicate sparse or only seasonal human occupation during the
117 Mesolithic and Neolithic (10,000–3800 cal BP) (Engel and Sobczak, 2012). Around 2000 cal BP human presence
118 increases in the region with stronghold settlements, animal husbandry and fishing (Kinder et al., 2019). Yet, the
119 area around Lake Jaczno remained isolated from human influences (Marcisz et al., 2020). Pollen and charcoal
120 data, and increased soil erosion indicate extensive forest clearance, forest fires and intensified agriculture,
121 suggesting permanent settlements and higher human impact since 500 cal BP, especially after 150 cal BP (1800
122 CE) (Kinder et al., 2019; Marcisz et al., 2020). The 1970s are marked by a regeneration of forest cover and a
123 significant increase of fertilizer use in agriculture (Poraj-Górska et al., 2017; Kinder et al., 2019), which markedly
124 increased lake primary production (Butz et al., 2016; Poraj-Górska et al., 2017).

125 **3.   Materials and methods**

126 Two parallel cores ca. 12.5 m long were retrieved in September 2017, using a UWITEC piston corer. The coring
127 site was located at the deepest part (24 m water depth) of the lake in the southern basin, which is protected from
128 direct external inputs (Fig. 1b). The cores were split lengthwise and then described following Schnurrenberger et
129 al. (2003) and the Munsell color chart (Munsell Color (Firm), 2010). Flood deposits and slumps were identified
130 based on grain size, mineral content, and sediment structure. First, the core halves were analysed using non-
131 destructive methods and further analytical measurements were performed after subsampling. The sampling interval
132 for LOI, CNS and dry-bulk density analysis was 10 cm (ca. 80-year resolution, discrete sampling). For the HPLC
133 and spectrophotometer analysis, 46 discrete samples (1–2 cm^3) were taken every ca. 30–35 cm (ca. 230 years
134 resolution) taking into account the HSI scanning data and optimization for the proxy-to-proxy calibration of the
135 HSI indices with spectrophotometer data (Butz et al., 2015). The top 10 cm (last ca. 50 years) were subsampled
136 continuously every 1 cm.
137
138 The chronology is based on 18 radiocarbon Accelerator Mass Spectrometry (AMS) dates on taxonomically
139 identified terrestrial plant macrofossils (Table 1) measured at the Laboratory for Radiocarbon Analysis at the
140 University of Bern. Samples with < 300 μg C were measured using the gas-source input of the MIni CArbon
141 DAting System (Szidat et al., 2014; Zander et al., 2020). The age–depth model was calculated using Bacon (rbacon
142 v. 2.4.2; Blaauw et al., 2020; Blaauw and Christeny, 2011) and the IntCal13 calibration curve (Reimer et al., 2013).
143 Event layers (>3 cm) and slumps were excluded from the age calculation (Fig. 2). According to changes in
144 lithology, we used model parameters that allowed for a higher sedimentation rate in the lowermost 137 cm (Fig.
145 2).
146
147 XRF scanning was performed at continuous 2 mm steps using an ITRAX μXRF core scanner (exposure time 20 s,
148 30 kV and 50 mA) equipped with a Cr-tube at the University of Bern. The results are given as counts (peak area).
149 From the detected elements, Ti was used as proxy for erosional input from the catchment, Ca as a proxy for
150 endogenic calcium carbonates, Si/Ti as a proxy for biogenic silica, S, Fe, Mn, and Mn/Fe as proxies of changing
151 redox conditions (Koinig et al., 2003; Croudace and Rothwell, 2015).
152
153 Hyperspectral imaging scanning (HSI) was performed on the freshly oxidized core halves using a Specim PFD-
154 CL-65-V10E camera (400 to 1000 nm spectral range; 2.8 nm spectral resolution). We used a spatial resolution of
155 ~68 μm per pixel with a spectral sampling of 1.57 nm. Data were processed using the ENVI software version 5.4

(Exelis Visual Information Solutions, Boulder, Colorado) following Butz et al. (2015). The relative absorption band depths (RABDs) were calculated based on spectral endmembers analysis in ENVI. The $RABD_{673}$ (spectral region 590–730 nm) was used to detect chlorophyll *a* and *b* and their diagenetic products (TChl) and served as a proxy for aquatic primary production (Leavitt and Hodgson, 2001). The $RABD_{845}$ (spectral region 790–895 nm) was used to detect total bacteriopheophytin *a* and *b* (*Bphe*) (Butz et al., 2015, 2016), which is a proxy for anoxia and meromixis as described in Makri et al. (2020). Bphe *a* and *b* is produced by anoxygenic phototrophic purple sulfur and non-sulfur bacteria that proliferate in illuminated anoxic habitats (Yurkov and Beatty, 1998; Madigan and Jung, 2009). Green sulfur bacteria produce bacteriochlorophyll *c*, *d* and *e*, which do not absorb in the $RABD_{845}$ range. Therefore, HSI-inferred Bphe reflects purple bacteria abundance.

The spectral indices were calibrated with absolute pigment concentrations of 46 selected sediment samples (1 cm^3) measured by spectrophotometry (Shimadzu UV-1800). Pigments were extracted using pure acetone. The supernatant was evaporated under nitrogen, and extracts were subsequently redissolved in 2 ml of pure acetone (method adapted from Schneider at al. 2018). For the calculation of Bphe concentrations, we used the molar extinction coefficient for Bphe *a* by Fiedor et al. (2002). For TChl, we applied the molar extinction coefficient for chlorophylls and chlorophyll derivatives by Jeffrey et al. (1975). The performance of the proxy-to-proxy linear regression models was assessed using the coefficient of determination (R^2) and the root mean square error of prediction (RMSEP) (Butz et al., 2015) run in R (R Core Team, 2015). The calibration model for TChl showed an R^2 of 0.91 (p < 0.001) and a RMSEP ~8 % (Fig. S1a). The calibration model for Bphe showed an R^2 of 0.95 (p < 0.001) and a RMSEP ~6 % (Fig. S1b). The Shapiro–Wilk and the Kolmogorov–Smirnov tests of the residuals show that they are most likely normally distributed, suggesting that inferences can be made with both models.

HPLC analysis was conducted on the same 46 samples used for the proxy-to-proxy calibration. Chlorophyll, chlorophyll derivatives and carotenoids were measured using ion pairing reverse-phase (Mantoura and Llewellyn, 1983; Hurley, 1988). The system used a UV-VIS detector set at 460 nm and 656 nm for carotenoids and chloropigments, respectively. The results were corrected for water content and expressed as nmol g OM^{-1} (Züllig, 1982; Guilizzoni et al., 1983; Lami et al., 1994). According to Jeffrey et al. (2011), Guilizzoni and Lami (2002), chlorophyll *a*, *ββ*-carotene, pheophytin *a*, and pheophytin *b* are considered as indicators of total algal biomass. Chlorophyll *b* and lutein are associated with green algae. *B*-carotene, dinoxanthin (pyrophytes), diadinoxanthin (siliceous algae), fucoxanthin (diatoms), diatoxanthin (chrysophytes) and alloxanthin (cryptophytes) are related to brown algae. Echinenone and zeaxanthin are associated to most taxa of blue–green algae, and myxoxanthophyll and canthaxanthin to colonial and filamentous cyanobacteria (Leavitt and Hodgson, 2001). K-myxol (4-keto-myxol-2'-methylpentoside) is associated with N-fixing cyanobacteria (*Anabaena flos-aquae*) (Kosourov et al., 2016). Pheophorbide *a* is a degradation product of Chl *a* transformed by microbial processes and used as an indicator of grazing (Bianchi and Findlay, 1991; Cartaxana et al., 2003). In the phototrophic bacteria community, BChl *a* is common to all anoxygenic phototrophic purple bacteria. Okenone (*Chromatium sp.*) is associated with purple sulfur bacteria (PSB), whereas spheroidene and spheroidenone (*Rhodopseudomonas sphaeroides*) are related to purple nonsulfur bacteria (PnSB). Both groups are able to oxidize sulfide. Yet, PSB store any S^0 formed intracellularly, whereas PnSB do so outside the cell (Madigan and Jung, 2009). The main difference between the two groups is that PSB are strong photoautotrophs, whereas PnSB are physiologically versatile and can grow well both phototrophically and in darkness via fermentation or anaerobic respiration (Madigan and Jung, 2009). *R.*

197 *sphaeroides* are also excellent N-fixing bacteria. Oxygen tolerance varies among species, with *R. sphaeroides*

198 being able to grow under vigorous aeration. Spheroidenone is produced by *R. sphaeroides* only when even small

199 amounts of oxygen are present (Züllig, 1989). Hence, the presence of spheroidenone is used as an indication of

200 better oxygen conditions, whereas the presence of spheroidene with parallel absence of spheroidenone is used as

201 an indication of meromictic conditions (Züllig, 1989; Guilizzoni and Lami, 2002). Isorenieratene is associated

202 with GSB (*Chlorobium sp.*). GSB have low light requirements and can cope with low light availability, occupying

203 deeper layers in stratified lakes (Montesinos et al., 1983). Hence, a dominance of GSB over PSB is used as an

204 indicator of a deeper oxic–anoxic boundary (Montesinos et al., 1983; Itoh et al., 2003).

205

206 Total organic carbon (TOC) was determined by Loss on Ignition (LOI; Heiri et al., 2001). Total carbon (TC) and

207 total nitrogen (TN) were measured with a CNS-Analyzer (Elementar vario EL cube). Total inorganic carbon (TIC)

208 was calculated by the difference between TC and TOC (Enters et al., 2010). The TOC/TN ratio was used to infer

209 changes in OM sources (Meyers, 2003). The lithogenic flux was calculated based on the residual calculation after

210 removing the organic matter and carbonate fraction by LOI.

211

212 Statistical analysis was performed in R (R Core Team, 2015). To define the sedimentary lithotypes we performed

213 an hierarchical unconstrained clustering on the geochemical proxies (XRF data: Ti, Ca, Si/Ti, Si, S, Fe, Mn, Mn/Fe;

214 HSI: TChl, Bphe; TOC, TIC, TN, TOC/TN, Fig. 3) using the Euclidean distance matrix and the ward.D2 clustering

215 method (Murtagh and Legendre, 2014). On the same dataset, we performed a PCA analysis with the samples

216 grouped based on the unconstrained clustering to investigate the relationships between the lithotypes and the

217 geochemical variables (Fig. S2). The data were log transformed and scaled before statistical analysis. We

218 performed a redundancy analysis (RDA) using the Vegan package (Oksanen et al., 2016) in R to relate the pigment

219 matrix i.e HPLC- and HSI-inferred pigment concentrations (Hellinger-transformed variables) to the environmental

220 variables i.e. temperature (Heikkilä and Seppä, 2010), arboreal pollen (AP), non-arboreal pollen (NAP) (Kinder et

221 al., 2019; Marcisz et al., 2020) and lithogenic flux (log transformed variables). The elements were plotted using

222 scaling 2 (see Borcard et al., 2011, pp. 166–167). This analysis was followed by a permutation test in R to test for

223 significance in the redundancy analysis (Legendre and Legendre, 1998; Borcard et al., 2011). The zones of pigment

224 data were defined by constrained clustering using the Bray distance and ward.D2 linkage method in R.

225 **4.   Results and interpretation**

226 **4.1   Chronology**

227 The age–depth model (Fig. 2) reveals a basal age of ca. 9500 cal BP. The model shows a stationary distribution,

228 matching prior and posterior accumulation rates, and a smooth sediment accumulation as indicated by its memory

229 or variability (Fig. 2). Three radiocarbon samples (Fig. 2, in red) have calibrated ages that do not fit with the 95 %

230 confidence interval. Based on the lithology and the much older ages, these samples were considered as containing

231 reworked carbon and were excluded from the Bacon model. The sediment sequence is entirely laminated

232 throughout the Holocene showing regular continuous sedimentation without any hiatus. In the lowermost section

233 (1257–1120 cm), sedimentation rates (SR) are relatively high (0.5 cm y^{-1}) and the mean age error (95% confidence

234 interval) is ca. ±160 years. Numerous event layers and slumps characterize the part between 1120 cm and 800 cm

235 where the SR is ca. 0.2 cm y^{-1} and the mean age error is ca. ±200 years. From 800 cm to the top, the sediment is

236 continuously varved and the SR is 0.1 cm y^{-1} (0.2 cm y^{-1} in the last 500 years). The mean age error in this section

237 is ca. ±140 years. The ages at the top 10 cm of the core (data shown in Fig 4b) were calculated by extrapolation of

238 the radiocarbon chronology to the sediment surface. A stratigraphic correlation with the ^{210}Pb dated cores from

239 Butz et al. (2016) showed an age error of ±5 years for this section.

240 **4.2   Lithotypes and biogeochemical proxies**

241 Figure 3 shows the biogeochemical data that defined four sedimentary lithotypes A–D. Fig. S3 (supplementary

242 material) shows the RGB images and the biogeochemical composition of selected close-ups within the sediment

243 sequence. Lithotype A and B appear in segments between ca. 9500–6800 cal BP (Fig. 3). Lithotype A, at the

244 bottom part (9500–9200 cal BP), consists of light greenish grey (GLEY 2 7/2) fine sand and continues with pale

245 yellow (2.5Y 7/3) and grey (2.5Y 5/1) laminations with light greenish grey silty lenticular bedding. This part is

246 characterized by high detrital inputs (Ti, lithogenic flux), moderate carbonate content (Ca, TIC), low production

247 and biogenic silica (HSI-TChl, Si/Ti) and low TOC. Low HSI-Bphe and S, and higher Mn/Fe ratio indicate

248 effective oxygenation of bottom waters. From ca. 9200–8500 cal BP, lithotype B is introduced and is characterized

249 by slightly higher production (HSI-TChl) and biogenic silica (Si/Ti); carbonates (TIC, Ca), TOC and TN contents

250 increase, whereas higher S, Fe and HSI-Bphe, and lower Mn/Fe ratio indicate the development of anoxic (sulfidic)

251 conditions. Between ca. 8500–6800 cal BP, lithotype A continues with varved sediments; starting with biogenic

252 pale yellow (2.5Y 7/3) and grey (2.5Y 5/1) varves with intercalated reddish brown (2.5YR 5/4) and reddish black

253 (2.5YR 2.5/1) laminations rich in clastic material and iron oxides. In the second half of this part, varves are less

254 well-preserved with several intercalated clastic-rich laminations. Based on color, layer thickness, and grain size

255 we interpret these intercalated layers as event (flood) deposits. In this period, lithotype A is characterized by high

256 detrital input (Ti, lithogenic flux); primary production (HSI-TChl) remains unchanged and carbonates (Ca, TIC)

257 show increased variability. Biogenic silica (Si/Ti), TOC and Fe slightly decrease. S decreases, HSI-Bphe is very

258 low or absent and Mn/Fe increases, suggesting better oxygen conditions.

259

260 Lithotype C occurs between ca. 6800–500 cal BP and consists mainly of light grey (2.5YR) and dark grey (2.5YR

261 4/1) fine biogenic varves, with some dispersed event layers that occur only at the beginning of this period until ca.

262 6000 cal BP. This period is characterized by low erosional input (Ti, lithogenic flux), gradually increasing

263 production (HSI-TChl) and TOC content, fluctuating biogenic silica (Si/Ti) and constantly high carbonates content

264 (Ca, TIC). S counts are minimal. HSI-Bphe is mostly present suggesting the development of anoxic conditions in

265 the hypolimnion. Mn/Fe seems to fluctuate, with higher values when HSI-Bphe is lower and vice versa.

266

267 Lithotype D occurs from ca. 500 cal BP to the present and consists of biogenic pale yellow (2.5Y 7/3), grey (2.5Y

268 5/1) and dark grey (2.5Y 4/1) calcareous biogenic varves. This period is characterized by instances of higher

269 detrital input (Ti) and several intercalated event (flood) layers. Mn counts also increase. Primary production (HSI-

270 TChl), TOC and TN reach maximum levels, whereas biogenic silica and carbonates (Ca, TIC) decrease. HSI-Bphe

271 reach maximum values at the top suggesting persistent anoxia in this part. The Mn/Fe ratio and HSI-Bphe show

272 opposite fluctuations indicating phases of better oxygen conditions when Bphe is absent.

4.3 HPLC pigment stratigraphy

Figure 4 presents the pigment dataset of individual chlorophylls and carotenoids measured by HPLC in the Holocene (Fig. 4a), and for the last 50 years (Fig. 4b). The pigments are grouped according to their taxonomic relation and the zones are defined by constrained clustering, which yielded boundaries that are similar to those of the sediment lithotypes (Fig. 3).

In zone I (ca. 9500–9200 cal BP), pigment concentrations are very low. Chromophytes are more abundant than green algae, especially cryptophytes (alloxanthin) and chrysophytes (fucoxanthin). Blue–green algae (echinenone, zeaxanthin) are present in low concentrations. Grazing (pheophorbide *a*) is low. In the purple bacteria group, *Chromatium* species (okenone, PSB) are absent, whereas *R. sphaeroides* (spheroidene and spheroidenone, PnSB) are both present in low concentrations. *Chlorobium sp.* (isorenieratene, GSB) are present in traces.

In zone II (ca. 9200–6700 cal BP), pigment concentrations increase overall. Green algae (chlorophyll *b*, lutein) still have low concentrations, whereas chromophytes (*β*-carotene) become more abundant especially pyrophytes (dinoxanthin) and chrysophytes (diatoxanthin) that show a distinctive local maximum around 7300 cal BP. Colonial filamentous cyanobacteria (canthaxanthin) appear in this zone. Grazing (pheophorbide *a*) starts increasing around 8300 cal BP. *Chromatium sp.* (okenone, PSB) is mostly absent. *R. sphaeroides* (spheroidene and spheroidenone, PnSB) have moderate concentrations, whereas *Chlorobium sp.* (isorenieratene, GSB) reach a maximum around 7300 cal BP.

In zone III (6700–500 cal BP), most pigments concentration increase gradually. Green algae (chlorophyll *b*) increase significantly. Chromophytes remain abundant. Diatoms and other siliceous algae (diadinoxanthin, fucoxanthin), and cryptophytes (alloxanthin) show a local maximum around 2000 cal BP. Blue–green algae (echinenone, zeaxanthin) increase gradually. More colonial filamentous cyanobacteria (myxoxanthophyll) appear around 2300 cal BP and, together with zeaxanthin, reach a maximum around 2000 cal BP. N-fixing cyanobacteria (k-myxol) appear at ca. 5000 cal BP. *Chromatium sp.* (okenone, PSB) appear in this zone and increase gradually. *R. sphaeroides* (spheroidene and spheroidenone, PnSB) also show a gradual increase, whereas *Chlorobium sp.* (isorenieratene, GSB) decrease to minimum concentrations.

Zone IV (500 cal BP to present), is characterized by a further gradual increase of most pigments, reaching unprecedented maximum concentrations at the top. In more detail, Fig. 4b shows the distribution of pigment concentrations in the last 50 years. Most pigments reach maximum values around 1997 CE. *Chromatium sp.* (okenone, PSB) have high concentrations, whereas *R. sphaeroides* are present producing only spheroidene and almost no spheroidenone. *Chlorobium sp.* (isorenieratene, GSB) show only trace concentrations around 1997 CE.

4.4 The relationships between land use, temperature, and pigment stratigraphy

We applied a redundancy analysis (RDA) to examine the response of our HPLC- and HSI-inferred pigment dataset to land use changes (arboreal pollen: AP, and non-arboreal pollen: NAP; Kinder et al., 2019; Marcisz et al., 2020), annual mean temperature variability (Heikkilä and Seppä, 2010) and catchment surface processes (lithogenic flux). Figure 5 shows the RDA ordination output in a triplot with the explanatory variables (in blue) and response (in red) variables, as well as the samples divided into the four distinct zones defined by constrained clustering (see

313 Sect. 4.3). The numerical output shows that the first two axis (RDA 1 20.95 % and RDA 2 11.25 %) explain 36 %
314 of the variation (unadjusted values). The R^2_{adj} for the constrained ordinations suggests that this model explains ca.
315 29 % of the variation in the data. The permutation test on the unconstrained ordinations indicates that the first two
316 axis are significant (p<0.001; Table S1) and represent the data adequately.

317

318 The RDA triplot (Fig. 5) shows that AP and NAP play an important role in the distribution of the pigment data
319 along the first axis (RDA 1). Lithogenic flux and temperature drive pigment variability along the second axis
320 (RDA 2). Lithogenic flux is strongly correlated with siliceous algae (fucoxanthin, diadinoxanthin) and blue–green
321 algae (echinenone), as well as enhanced aquatic primary production (HSI-TChl) by green algae (lutein) and
322 cryptophytes (alloxanthin, β-carotene). Lithogenic flux is clearly anticorrelated with PSB (okenone, HSI-Bphe)
323 and Chl a. AP is mainly correlated with GSB pigments (isorenieratene) indicating a deeper oxic–anoxic boundary,
324 and PnSB (spheroidene and spheroidenone) that suggest a more effective oxygenation of the water column. AP is
325 also correlated with variables indicating the presence of chromophyte (brown) algae, pyrophytes (dinoxanthin),
326 chrysophytes (diatoxanthin), as well as some blue–green algae (zeaxanthin). Higher lithogenic input and AP drive
327 pigment variability in zones I and II. Temperature seems to be correlated with higher production of some green
328 algae (Chl b, pheophytin b), increased cyanobacteria abundance ($\beta\beta$-carotene, β-carotene) and colonial-
329 filamentous cyanobacteria (myxoxanthophyll, canthaxanthin). Temperature seems to drive pigment variability
330 mainly in zone III. NAP is correlated with PSB production (BChl a, HSI-Bphe and okenone), overall higher
331 primary production (Chl a, pheophytin a), higher grazing (pheophorbide a), and N-fixing cyanobacteria (k-myxol).
332 NAP drives pigment variability in zone IV.

333 **5.   Discussion**

334 **5.1   Combining sedimentological and biogeochemical data to infer past lake production and bottom**
335 **water oxygenation**

336 The 12.5 m long and almost entirely varved sediment record of Lake Jaczno continuously spans the last ca. 9500
337 cal yr BP (Fig. 2). The chronology is robust and exclusively based on terrestrial macrofossils. The lithology of
338 Lake Jaczno (Fig. 3) revealed the deposition of frequent event layers between 8500–7000 cal BP, which likely
339 reflect a regional catchment/climatic signal as similar features have been observed, for the same period, in the
340 nearby Lake Szurpiły (Kinder et al., 2020). The physical characteristics of the catchment favored the transport of
341 lithogenic material into the lake (Fig. 3), thereby possibly affecting the density stratification, light availability, and
342 subsequently the phototrophic community dynamics. A proper assessment of these changes requires high-
343 resolution data that is impossible to reach using HPLC data alone. Yet, the combination of high-resolution (μm-
344 scale) calibrated HSI bulk data for TChl and Bphe, combined with scanning XRF and compound specific HPLC
345 data, provides a unique opportunity for paleoproduction and paleooxygenation reconstructions at sub-seasonal
346 scale for multi-millennial-long records (Butz et al., 2017; Makri et al., 2020). This approach is directly applicable
347 to diverse lacustrine (Butz et al., 2017; Schneider et al., 2018; Makri et al., 2020; Sanchini et al., 2020) and
348 potentially marine environments (Hubas et al., 2011, 2013) with uncertain past redox state changes.

349

350 The calibration of the RABD$_{673}$ and RABD$_{845}$ to absolute pigment concentrations of green pigments (chlorophylls
351 and diagenetic products) and Bphe (a and b) respectively, revealed robust calibration statistics (Fig. S1,
352 supplementary material) with very low uncertainties (ca. 6–8 %) comparable to other studies (Butz et al., 2017;

353 Schneider et al., 2018; Makri et al., 2020; Sanchini et al., 2020). Between ca. 9200 and 7000 cal BP, the calibration
354 model of the $RABD_{673}$ for green pigments calculates negative concentrations (Fig. 3). This offset can be produced
355 by matrix effects, i.e. the variability of the reflectance of the sediment matrix or substances that absorb in the same
356 range as chlorophylls and their diagenetic products (590–730 nm) (Makri et al., 2020). Interestingly, GSB
357 (isorenieratene) peak between 9200 and 7000 cal BP (Fig. 4). GSB contain bacteriochlorophyll *c*, *d*, and *e* that
358 absorb in the same range as chlorophylls and chlorophyll derivatives (Oren, 2011). This could indicate that a part
359 of the $RABD_{673}$ calibration error may be due to the increased GSB abundance. Nonetheless, the calibration
360 statistics reveal an overall error of less than 8 %.

361 **5.2   Holocene production dynamics and chemocline evolution**

362 The presence of anoxygenic sulfur bacteria throughout our record, combined with chlorophylls, carotenoids and
363 geochemical evidence, suggests that euxinic conditions prevailed in Lake Jaczno for most of the past 9500 years.
364 Nonetheless, the changing composition of photosynthetic sulfur bacteria indicates persisting but variable euxinia.
365 Figure 6 summarizes the Holocene evolution of the relative abundance of PSB, PnSB and GSB, *Chromatium*
366 (okenone) and *Clorobium* (isorenieratene), the content of spheroidene and spheroidenone pigments produced by
367 *R. sphaeroides*, and the high-resolution calibrated HSI-TChl and Bphe, with respect to lithogenic flux, climate
368 variability (annual mean temperature; Heikkilä and Seppä, 2010) and human impact (land use and vegetation
369 cover; Kinder et al., 2019; Marcisz et al., 2020).

370 **5.2.1   Low trophic levels with a deep oxic–anoxic boundary**

371 In the period from 9500 to 6700 cal BP, which corresponds to pigment zones I and II, the phototrophic bacteria
372 population is dominated by GSB (Fig. 6). A small percentage of PnSB (*R. sphaeroides*) is present and seems to
373 produce both spheroidene and spheroidenone during this time. *Chromatium* (okenone, PSB) is almost completely
374 absent. Considering that *R. sphaeroides* produces spheroidenone only when even small amounts of oxygen is
375 present (Züllig, 1989) we suggest that, in this period, euxinic conditions were already present but the strength or
376 extent of anoxia was likely weak. HSI-Bphe that corresponds to purple bacteria is very low. Anoxia is mainly a
377 function of lake stratification and productivity. HSI-TChl, which indicates total primary production, is still at low
378 levels (Fig. 6). Indeed, the stratigraphy of individual pigments indicates low to moderate in-lake production, which
379 mainly consists of chromophyte (brown) algae and some colonial cyanobacteria (canthaxanthin) (Fig. 4), which is
380 also confirmed in the RDA analysis (Fig. 5). Brown siliceous algae are well adapted and tolerant algae species that
381 thrive in oligotrophic conditions in symbiosis with other algae species and bacteria (Bird and Kalff, 1986; Wetzel,
382 2001). Similar observations of algae composition were made in Lake Peipsi (Tõnno et al., 2019; Estonia) and Lake
383 Lazduny (Sanchini et al., 2020; NE Poland).

384

385 Temperature gradually increased and a closed forest canopy with pine/birch and later elm/hazel/alder persisted in
386 the catchment (Fig. 6) (Gałka, 2014). These provided shelter from wind and increased the nutrient pools in the
387 catchment soils (Bajard et al., 2017). The closed forest canopy, combined with the deep and relatively small basin
388 (relative depth 3.01 %), favors the establishment of a naturally anoxic hypolimnion (Zolitschka et al., 2015). Yet,
389 it seems that enhanced permanent stratification was still not established in the lake. This phase of GSB dominance
390 corresponds to a period of high lithogenic flux or high-energy sedimentation (Fig. 3, 6), as confirmed in the RDA
391 analysis (Fig. 5). Turbidity currents and underflows can increase turbidity and nutrient availability, but can also

392   cause sporadic ventilation of bottom waters. Higher suspended matter and/or algal growth would decrease light
393   availability in the oxic–anoxic boundary. Since GSB and PnSB are more tolerant to low light intensities than PSB
394   (Biebl and Pfennig, 1978; Parkin and Brock, 1980; Madigan and Jung, 2009), a dominance of GSB and presence
395   of spheroidene and spheroidenone in the sediments is expected under these conditions. Similar observations were
396   made in Lake Cadagno (Wirth et al., 2013). GSB often inhabit the lowermost part of stratified water bodies due to
397   their efficient light capture (Manske et al., 2005; Imhoff, 2014). Higher abundance of GSB could also indicate a
398   deep oxic–anoxic boundary in the lake (Itoh et al., 2003; Antoniades et al., 2009).

399   **5.2.2   Gradually increasing trophy levels with a shallower oxic–anoxic boundary**

400   The period from 6700 to 500 cal BP, which corresponds to pigment zone III, is characterized by a gradual shift in
401   the phototrophic bacterial community to higher PSB abundance, especially after ca. 2000 cal BP (Fig. 6). GSB are
402   present, inhabiting the anoxic layers below PSB and seem to fluctuate as a function of the primary production in
403   the oxic layer (HSI-TChl) and related light availability (Montesinos et al., 1983). When production was higher in
404   the oxic layers, *Chromatium* (okenone, PSB) increased and *Chlorobium* (isorenieratene, GSB) decreased. This is
405   also confirmed by the individual pigment stratigraphy (Fig. 4). Green algae (chlorophyll *b*, lutein) and N-fixing
406   cyanobacteria (k-myxol) increase markedly since ca. 5500 cal BP, indicating a higher lake trophy than before,
407   driven most probably by lake ontogeny and a gradual increase of nutrient availability. The appearance of N-fixing
408   cyanobacteria at that time agrees with this interpretation. Prolonged periods of anoxia leading to intense recycling
409   of phosphorous from the sediments would decrease the N:P ratio in the water column promoting nitrogen fixation
410   by N-fixing algae (Howarth et al., 1999; Vitousek et al., 2002). Similar trends in lake trophy evolution are reported
411   from nearby Lake Szurpiły (Kinder et al., 2019) and Lakes Albano and Peipsi (Lami et al., 2000; Guilizzoni and
412   Lami, 2002; Tõnno et al., 2019). An increase of *Chromatium* (okenone, PSB) over *Chlorobium* (isorenieratene,
413   GSB) with increasing lake trophy has been reported from other lakes, e.g. Lake Albano in Italy (Lami et al., 1994),
414   Little Round Lake in Canada (Brown et al., 1984), and Lake Hamana in Japan (Itoh et al., 2003). *R. sphaeroides*
415   (PnSB) are also present producing both spheroidene and spheroidenone, suggesting phases of effective aeration of
416   bottom waters (Züllig, 1989).
417
418   The catchment is continuously densely forested and human impact is very low (Fig. 6). The RDA analysis points
419   to a temperature driven pigment variability in this zone, but mainly for cyanobacteria abundance (Fig. 5).
420   Cyanobacteria can benefit from higher water temperature, yet nutrient inputs have in most cases a much stronger
421   and synergetic effect (Lürling et al., 2018). Temperature variability did not seem to have affected lake stratification
422   directly. However, seasonality, precipitation and windiness play an important role in lake circulation and are not
423   reflected in the annual mean temperature variability. Hence, the role of climate may be underestimated. The oxic–
424   anoxic stratification was enhanced in this period but permanent perennial anoxia was still not established as
425   indicated also by the low HSI-Bphe concentrations. The increase in PSB abundance suggests a shallower oxic–
426   anoxic boundary (Itoh et al., 2003). It appears that during most of the Holocene, anoxia was largely influenced by
427   primary production and lithogenic flux. The case of Lake Jaczno is different from e.g Lake Łazduny (Masurian
428   Lake District, NE Poland; Sanchini et al., 2020), where erosional input is negligible and anoxia was mainly a
429   function of primary production and forest cover.

5.2.3   20th century eutrophication, shallow oxic–anoxic boundary and meromixis

In the period from 500 cal BP to the present, which corresponds to pigment zone I, phototrophic sulfur bacteria composition changed to an almost complete dominance of purple bacteria (Fig. 6). Between 500–200 cal BP, HSI-Bphe and the absolute concentrations of PSB (okenone,) and PnSB (spheroidene and spheroidenone) are at a minimum, but dominate the phototrophic bacteria community since GSB are completely absent (Fig. 4, 6). Lake production (HSI-TChl) also decreases while lithogenic flux increases (Fig. 6). These suggest an oxic rather than anoxic phase during this period, with some intervals of weak euxinia. Increased Mn accumulation during this time (Fig. 3) supports the indications of rather oxygenated bottom waters.

Between 200 cal BP to the present, when human impact starts to increase in the catchment (Fig. 5), PSB increase as well. Presence of spheroidene and only trace concentrations of spheroidenone (PnSB) and isorenieratene (GSB) suggest increasing and gradually persisting anoxia. Intensive agriculture in the last 100 years and use of fertilizers, combined with exceptionally warm summers after 1990 CE (Czernecki and Miętus, 2017; IMGW-PIB, 2017) increased primary production (HSI-TChl) substantially to unprecedented levels in the 1990s, relative to the Holocene baseline. This is also reflected in the individual pigment stratigraphy (Fig. 4). Bphe reaches maximum levels suggesting persisting anoxia and mostly meromictic conditions in the lake, especially since the 1970s when gradual afforestation in the catchment is observed. This is also supported by the HPLC-inferred composition of phototrophic bacteria (Fig. 3).

In this period, the high-resolution HSI-Bphe record indicates that the intervals of lowest AP in the catchment coincide with absence of Bphe, indicating oxic bottom waters. Bphe increases again only when AP and the tree canopy recovers (Fig. 6), with a parallel absence of spheroidenone (PnSB), suggesting meromictic conditions. Butz et al. (Butz et al., 2016, 2017) showed that these intervals of low AP and low or absent Bphe in the sediments were accompanied by strong pulses of terrigenous material from the catchment. The role of human impact with regard to anoxia and interrelated catchment processes (deforestation/afforestation and nutrient inputs) has also been shown in other lakes with diverse timing of human impact onset. For example, Lake Moossee (Makri et al., 2020) and Soppensee (Lotter, 1999) on the Swiss Plateau, Lakes Albano and Nemi in Italy (Guilizzoni et al., 2002), Lake Zazari in Greece (Gassner et al., 2020) with an early Mid-Holocene human impact, and Lake Szurpiły (Kinder et al., 2019) in the vicinity of Lake Jaczno with a late human impact, mainly in the last 500 years.

6.   Conclusions

In this study, we used a multiproxy approach, combining high-resolution HSI pigment data with lower resolution HPLC-inferred concentrations of specific algal pigments, and geochemical data to investigate algal community composition and its relationship with aquatic production and water column oxygenation in a 9500-years sediment record from NE Poland. Land use changes, vegetation cover and climate variability were also taken into account. Our aim was to examine factors that determine trophic state changes and lake stratification, in a lake system with stable catchment vegetation and low human impact until very recent times.

The Holocene sedimentary pigment and geochemical record of Lake Jaczno revealed distinct changes in lake trophy and stratification states, mainly driven by the catchment evolution, lithogenic flux, nutrient input and subsequent increase in primary production. The lake had a first phase (9500–6700 cal BP) of low production that

469 consisted mainly of brown algae in the oxic zone, yet an early immediate establishment of weak euxinic conditions

470 in a deep water column dominated by GSB in its anoxic zone. Increased suspended loads, turbidity currents and

471 underflows seem to have increased turbidity and restricted the proliferation of PSB at the deep oxic–anoxic

472 boundary. Between 6700–500 cal BP, primary production increased gradually with higher contributions of green

473 algae and cyanobacteria, following lake ontogeny in a continuously densely forested catchment. The oxic–anoxic

474 boundary became gradually shallower with a shift from GSB to PSB. The composition of phototrophic bacteria

475 and the presence of spheroidene and spheroidenone (PnSB) in the sediments suggest pronounced yet intermittent

476 euxinia in the lake. Between 500 cal BP to the present, lake trophy increases dramatically, especially in the last

477 100 years, due to intensified human impact. Eutrophication accompanied by catchment deforestation and

478 subsequent afforestation after land abandonment were the main driving forces for the establishment of permanently

479 anoxic and meromictic conditions in the modern lake.

480

481 This study highlights the great potential of calibrated and validated HSI measurements combined with HPLC data.

482 Lake Jaczno provided a rare site to explore the mechanisms that can potentially induce changes in lake mixing,

483 production and sustained bottom water anoxia in times from minimum to intensive human impact, in a naturally

484 stratified lake system. Our findings, together with findings from other lakes across Europe, can greatly expand our

485 understanding on these major environmental problems while providing a tailored toolset for implementing

486 effective remediation techniques in the future.

487 **Data availability**

488 The data is available at BORIS https://doi.org/10.5194/bg-2020-362.

489 **Author contributions**

490 **Stamatina Makri**: Investigation, Data Curation, Formal analysis, Writing - Original Draft, Visualization. **Luyao
491 Tu:** Investigation, Writing - Review & Editing. **Andrea Lami:** Investigation, Writing - Review & Editing.
492 **Wojciech Tylmann:** Writing - Review & Editing. **Hendrik Vogel:** Writing - Review & Editing, **Martin
493 Grosjean:** Conceptualization, Methodology, Writing - Review & Editing, Supervision, Funding acquisition.

494 **Competing interests**

495 The authors declare that they have no conflict of interest.

496 **Acknowledgments**

497 This study was funded by the Hans Sigrist Stiftung and the Swiss National Science Foundation Grants (SNF

498 200021_172586). We thank Andre F. Lotter, Willi Tanner, Paul Zander and Maurycy J Żarczyński for their help

499 during field work. We thank Petra Boltshauser-Kaltenrieder for plant macrofossils identification. Further, we

500 acknowledge Daniela Fischer and Patrick Neuhaus for their assistance in the lab.

501   **References**

502   Adrian, R., O'Reilly, C. M., Zagarese, H., Baines, S. B., Hessen, D. O., Keller, W., Livingstone, D. M.,

503   Sommaruga, R., Straile, D., Van Donk, E., Weyhenmeyer, G. A. and Winder, M.: Lakes as sentinels of climate

504   change, Limnol. Oceanogr., 54(6 PART 2), 2283–2297, doi:10.4319/lo.2009.54.6_part_2.2283, 2009.

505   Amann, B., Lobsiger, S., Fischer, D., Tylmann, W., Bonk, A., Filipiak, J. and Grosjean, M.: Spring temperature

506   variability and eutrophication history inferred from sedimentary pigments in the varved sediments of Lake

507   Zabińskie, north-eastern Poland, AD 1907-2008, Glob. Planet. Change, 123(PA), 86–96,

508   doi:10.1016/j.gloplacha.2014.10.008, 2014.

509   Antoniades, D., Veillette, J., Martineau, M. J., Belzile, C., Tomkins, J., Pienitz, R., Lamoureux, S. and Vincent,

510   W. F.: Bacterial dominance of phototrophic communities in a High Arctic lake and its implications for

511   paleoclimate analysis, Polar Sci., 3(3), 147–161, doi:10.1016/j.polar.2009.05.002, 2009.

512   Bajard, M., Poulenard, J., Sabatier, P., Develle, A. L., Giguet-Covex, C., Jacob, J., Crouzet, C., David, F.,

513   Pignol, C. and Arnaud, F.: Progressive and regressive soil evolution phases in the Anthropocene, Catena, 150,

514   39–52, doi:10.1016/j.catena.2016.11.001, 2017.

515   Battarbee, R. W. and Bennion, H.: Using palaeolimnological and limnological data to reconstruct the recent

516   history of European lake ecosystems: introduction, Freshw. Biol., 57(10), 1979–1985, doi:10.1111/j.1365-

517   2427.2012.02857.x, 2012.

518   Bennion, H. and Simpson, G. L.: The use of diatom records to establish reference conditions for UK lakes

519   subject to eutrophication, J. Paleolimnol., 45(4), 469–488, doi:10.1007/s10933-010-9422-8, 2011.

520   Bianchi, T. S. and Findlay, S.: Decomposition of Hudson estuary macrophytes: Photosynthetic pigment

521   transformations and decay constants, Estuaries, 14(1), 65–73, doi:10.2307/1351983, 1991.

522   Biebl, H. and Pfennig, N.: Growth yields of green sulfur bacteria in mixed cultures with sulfur and sulfate

523   reducing bacteria, Arch. Microbiol., 117(1), 9–16, doi:10.1007/BF00689344, 1978.

524   Bird, D. F. and Kalff, J.: Bacterial Grazing by Planktonic Lake Algae, Science (80-.)., 231(4737), 493–495,

525   doi:10.1126/science.231.4737.493, 1986.

526   Blaauw, M. and Christeny, J. A.: Flexible paleoclimate age-depth models using an autoregressive gamma

527   process, Bayesian Anal., 6(3), 457–474, doi:10.1214/11-BA618, 2011.

528   Blaauw, M., Christen, J. A., A. Aquino L., M., Esquivel Vazquez, J., Gonzalez V., O. M., Belding, T., Theiler,

529   J., Gough, B. and Karney, C.: Age-Depth Modelling using Bayesian Statistics, 2020.

530   Borcard, D., Gillet, F., Legendre, P., Borcard, D., Gillet, F. and Legendre, P.: Canonical Ordination, in

531   Numerical Ecology with R, pp. 153–225, Springer, New York, NY., 2011.

532   Brown, S. R., McIntosh, H. J. and Smol, J. P.: Recent paleolimnology of a meromictic lake: Fossil pigments of

533   photosynthetic bacteria, SIL Proceedings, 1922-2010, 22(3), 1357–1360, doi:10.1080/03680770.1983.11897499,

534   1984.

535   Butz, C., Grosjean, M., Fischer, D., Wunderle, S., Tylmann, W. and Rein, B.: Hyperspectral imaging

536   spectroscopy: a promising method for the biogeochemical analysis of lake sediments, J. Appl. Remote Sens.,

537   9(1), 096031, doi:10.1117/1.JRS.9.096031, 2015.

538   Butz, C., Grosjean, M., Poraj-Górska, A., Enters, D. and Tylmann, W.: Sedimentary Bacteriopheophytin a as an

539   indicator of meromixis in varved lake sediments of Lake Jaczno, north-east Poland, CE 1891–2010, Glob.

540   Planet. Change, 144, 109–118, doi:10.1016/j.gloplacha.2016.07.012, 2016.

541   Butz, C., Grosjean, M., Goslar, T. and Tylmann, W.: Hyperspectral imaging of sedimentary bacterial pigments: a

542 1700-year history of meromixis from varved Lake Jaczno, northeast Poland, J. Paleolimnol., 58(1), 57–72,

543 doi:10.1007/s10933-017-9955-1, 2017.

544 Cartaxana, P., Jesus, B. and Brotas, V.: Pheophorbide and pheophytin a-like pigments as useful markers for

545 intertidal microphytobenthos grazing by Hydrobia ulvae, Estuar. Coast. Shelf Sci., 58(2), 293–297,

546 doi:https://doi.org/10.1016/S0272-7714(03)00081-7, 2003.

547 Costa, K. M., Russell, J. M., Vogel, H. and Bijaksana, S.: Hydrological connectivity and mixing of Lake Towuti,

548 Indonesia in response to paleoclimatic changes over the last 60,000years, Palaeogeogr. Palaeoclimatol.

549 Palaeoecol., 417, 467–475, doi:https://doi.org/10.1016/j.palaeo.2014.10.009, 2015.

550 Croudace, I. W. and Rothwell, R. G.: Future Developments and Innovations in High-Resolution Core Scanning,

551 in Micro-XRF Studies of Sediment Cores. Developments in Paleoenvironmental Research, edited by I. Croudace

552 and R. Rothwell, pp. 627–647, Springer, Dordrecht., 2015.

553 Czernecki, B. and Miętus, M.: The thermal seasons variability in Poland, 1951–2010, Theor. Appl. Climatol.,

554 127(1), 481–493, doi:10.1007/s00704-015-1647-z, 2017.

555 Diaz, R. and Rosenberg, R.: Spreading Dead Zones and Consequences for Marine Ecosystems, Science, 321,

556 926–929, doi:10.1126/science.1156401, 2008.

557 Engel, M. and Sobczak, C.: Nie tylko archeologia. Interdyscyplinarne badania wielokulturowego zespołu

558 osadniczego w Szurpiłach na Suwalszczyźnie., Pruthenia, 7, 137–157 [online] Available from:

559 https://d1wqtxts1xzle7.cloudfront.net/33693318/Pruthenia_7_2012_Engel-C_Sobczak-

560 C_Nie_tylko_archeologia_Interdyscyplinarne_badania_w_Szurpilach.pdf?1400025472=&response-content-

561 disposition=inline%3B+filename%3DNie_tylko_archeologia_Interdyscyplinarne.pdf&, 2012.

562 Enters, D., Kirilova, E., Lotter, A. F., Lücke, A., Parplies, J., Jahns, S., Kuhn, G. and Zolitschka, B.: Climate

563 change and human impact at Sacrower See (NE Germany) during the past 13,000 years: A geochemical record,

564 J. Paleolimnol., 43(4), 719–737, doi:10.1007/s10933-009-9362-3, 2010.

565 Fiedor, J., Fiedor, L., Kammhuber, N., Scherz, A. and Scheer, H.: Photodynamics of the bacterlochlorophyll-

566 carotenoid system. 2. Influence of central metal, solvent and beta-carotene on photobleaching of

567 bacteriochlorophyll derivatives, Photochem. Photobiol., 76(2), 145–152, doi:https://doi.org/10.1562/0031-

568 8655(2002)076<0145:potbcs>2.0.co;2, 2002.

569 Friedrich, J., Janssen, F., Aleynik, D., Bange, H. W., Boltacheva, N., Çagatay, M. N., Dale, A. W., Etiope, G.,

570 Erdem, Z., Geraga, M., Gilli, A., Gomoiu, M. T., Hall, P. O. J. J., Hansson, D., He, Y., Holtappels, M., Kirf, M.

571 K., Kononets, M., Konovalov, S., Lichtschlag, A., Livingstone, D. M., Marinaro, G., Mazlumyan, S., Naeher, S.,

572 North, R. P., Papatheodorou, G., Pfannkuche, O., Prien, R., Rehder, G., Schubert, C. J., Soltwedel, T., Sommer,

573 S., Stahl, H., Stanev, E. V., Teaca, A., Tengberg, A., Waldmann, C., Wehrli, B. and Wenzhöfer, F.: Investigating

574 hypoxia in aquatic environments: Diverse approaches to addressing a complex phenomenon, Biogeosciences,

575 11(4), 1215–1259, doi:10.5194/bg-11-1215-2014, 2014.

576 Gächter, R.: Lake restoration. Why oxygenation and artificial mixing cannot substitute for a decrease in the

577 external phosphorus loading, Swiss J. Hydrol., 49(2), 170–185, doi:10.1007/BF02538501, 1987.

578 Gałka, M.: Pattern of plant succession from eutrophic lake to ombrotrophic bog in NE Poland over the last 9400

579 years based on high-resolution macrofossil analysis, Ann. Bot. Fenn., 51(1), 1–21, doi:10.5735/085.051.0101,

580 2014.

581 Gassner, S., Gobet, E., Schwörer, C., van Leeuwen, J., Vogel, H., Giagkoulis, T., Makri, S., Grosjean, M.,

582 Panajiotidis, S., Hafner, A. and Tinner, W.: 20,000 years of interactions between climate, vegetation and land

use in Northern Greece, Veg. Hist. Archaeobot., 29(1), 75–90, doi:10.1007/s00334-019-00734-5, 2020.

Guilizzoni, P. and Lami, A.: Paleolimnology: Use of Algal Pigments as Indicators, in Encyclopedia of Environmental Microbiology, edited by G. Bitton, pp. 2306–2317, John Wiley & Sons, Inc., 2002.

Guilizzoni, P., Bonomi, G., Galanti, G. and Ruggiu, D.: Paleolimnology: Relationship between sedimentary pigments and primary production: evidence from core analyses of twelve Italian lakes, in Hydrobiologia, vol. 103, edited by J. Meriläinen, P. Huttunen, and R. W. Battarbee, pp. 103–106, Kluwer Academic Publishers, The Hague, Netherlands., 1983.

Guilizzoni, P., Lami, A., Marchetto, A., Jones, V., Manca, M. and Bettinetti, R.: Palaeoproductivity and environmental changes during the Holocene in central Italy as recorded in two crater lakes (Albano and Nemi), Quat. Int., 88(1), 57–68, doi:10.1016/S1040-6182(01)00073-8, 2002.

Heikkilä, M. and Seppä, H.: Holocene climate dynamics in Latvia, eastern Baltic region: A pollen-based summer temperature reconstruction and regional comparison, Boreas, 39(4), 705–719, doi:10.1111/j.1502-3885.2010.00164.x, 2010.

Heiri, O., Lotter, A. F. and Lemcke, G.: Loss on ignition as a method for estimating organic and carbonate content in sediments: reproducibility and comparability of results, J. Paleolimnol., 25(1), 101–110, 2001.

Howarth, R. W., Chan, F. and Marino, R.: Do top-down and bottom-up controls interact to exclude nitrogen-fixing cyanobacteria from the plankton of estuaries? An exploration with a simulation model, Biogeochemistry, 46(1–3), 203–231, doi:10.1007/BF01007580, 1999.

Hubas, C., Jesus, B., Passarelli, C. and Jeanthon, C.: Tools providing new insight into coastal anoxygenic purple bacterial mats: Review and perspectives, Res. Microbiol., 162(9), 858–868, doi:10.1016/j.resmic.2011.03.010, 2011.

Hubas, C., Jesus, B., Ruivo, M., Meziane, T., Thiney, N., Davoult, D., Spilmont, N., Paterson, D. M. and Jeanthon, C.: Proliferation of purple sulphur bacteria at the sediment surface affects intertidal mat diversity and functionality, PLoS One, 8(12), 1–13, doi:10.1371/journal.pone.0082329, 2013.

Hurley, J. P.: Analysis of aquatic pigments by high performance liquid chromatography, J. Anal. Purif., 3, 12–16, 1988.

IMGW-PIB: Suwałki Meteorological Station, Inst. Meteorol. Water Manag. [online] Available from: https://danepubliczne.imgw.pl/#wprowadzenie, 2017.

Imhoff, J. F.: Biology of Green Sulfur Bacteria, eLS, doi:doi:10.1002/9780470015902.a0000458.pub2, 2014.

Itoh, N., Tani, Y., Nagatani, T. and Soma, M.: Phototrophic activity and redox condition in Lake Hamana, Japan, indicated by sedimentary photosynthetic pigments and molybdenum over the last ~250 years, J. Paleolimnol., 29(4), 403–422, doi:10.1023/A:1024407210928, 2003.

Jeffrey, S., Wright, S. and Zapata, M.: Phytoplankton Pigments., 2011.

Jeffrey, S. W. and Humphrey, G. F.: New spectrophotometric equations for determining chlorophylls a, b, c1 and c2 in higher plants, algae and natural phytoplankton, Biochem. und Physiol. der Pflanz., 167(2), 191–194, doi:10.1016/S0015-3796(17)30778-3, 1975.

Jenny, J.-P., Francus, P., Normandeau, A., Lapointe, F., Perga, M. E., Ojala, A., Schimmelmann, A. and Zolitschka, B.: Global spread of hypoxia in freshwater ecosystems during the last three centuries is caused by rising local human pressure, Glob. Chang. Biol., 22(4), 1481–1489, doi:https://doi.org/10.1111/gcb.13193, 2016a.

Jenny, J.-P., Normandeau, A., Francus, P., Taranu, Z. E., Gregory-Eaves, I., Lapointe, F., Jautzy, J., Ojala, A. E.

K., Dorioz, J.-M., Schimmelmann, A. and Zolitschka, B.: Urban point sources of nutrients were the leading cause for the historical spread of hypoxia across European lakes, Proc. Natl. Acad. Sci., 113(45), 12655–12660, doi:https://doi.org/10.1073/pnas.1605480113, 2016b.

Kinder, M., Tylmann, W., Bubak, I., Fiłoc, M., Gąsiorowski, M., Kupryjanowicz, M., Mayr, C., Sauer, L., Voellering, U. and Zolitschka, B.: Holocene history of human impacts inferred from annually laminated sediments in Lake Szurpiły, northeast Poland, J. Paleolimnol., 61(4), 419–435, doi:10.1007/s10933-019-00068-2, 2019.

Kinder, M., Tylmann, W., Rzeszewski, M. and Zolitschka, B.: Varves and mass-movement deposits record distinctly different sedimentation dynamics since the late glacial (Lake Szurpiły, northeastern Poland), Quat. Res. (United States), 93(1), 299–313, doi:10.1017/qua.2019.61, 2020.

Koinig, K. A., Shotyk, W., Lotter, A. F., Ohlendorf, C. and Sturm, M.: 9000 years of geochemical evolution of lithogenic major and trace elements in the sediment of an alpine lake - the role of climate, vegetation, and land-use history, J. Paleolimnol., 30(3), 307–320, 2003.

Kosourov, S., Murukesan, G., Jokela, J. and Allahverdiyeva, Y.: Carotenoid biosynthesis in calothrix sp. 336/3: Composition of carotenoids on full medium, during diazotrophic growth and after long-term H2 photoproduction, Plant Cell Physiol., 57(11), 2269–2282, doi:10.1093/pcp/pcw143, 2016.

Krzywicki, T.: The maximum ice sheet limit of the Vistulian Glaciation in northeastern Poland and neighbouring areas, Geol. Q., 46(2), 165–188, 2002.

Lami, A., Niessen, F., Guilizzoni, P., Masaferro, J. and Belis, C. A.: Palaeolimnological studies of the eutrophication of volcanic Lake Albano (Central Italy), J. Paleolimnol., 10(3), 181–197, 1994.

Lami, A., Guilizzoni, P. and Marchetto, A.: High resolution analysis of fossil pigments, carbon, nitrogen and sulphur in the sediment of eight European Alpine lakes: the MOLAR project, edited by A. Lami, N. Cameron, and A. Korhola, J. Limnol., 59(1), 15–28, 2000.

Leavitt, P. R.: A review of factors that regulate carotenoid and chlorophyll deposition and fossil pigment abundance, J. Paleolimnol., 9, 109–127, 1993.

Leavitt, P. R. and Hodgson, D.: Sedimentary Pigments, in Tracking Environmental Change Using Lake Sediments, vol. 3, edited by J. Smol, H. Birks, and W. Last, pp. 295–325, Kluwer, Dordrecht., 2001.

Legendre, P. and Legendre, L.: Numerical ecology. 2nd, Amsterdam., 1998.

Little, J. L., Quinlan, R., Smol, J. P. and Hall, R. I.: Past trophic status and hypolimnetic anoxia during eutrophication and remediation of Gravenhurst Bay, Ontario: Comparison of diatoms, chironomids, and historical records, Can. J. Fish. Aquat. Sci., 57(2), 333–341, doi:10.1139/f99-235, 2000.

Lotter, A. F.: Late-glacial and Holocene vegetation history and dynamics as shown by pollen and plant macrofossil analyses in annually laminated sediments from Soppensee, central Switzerland, Veg. Hist. Archaeobot., 8(3), 165–184, doi:10.1007/BF02342718, 1999.

Lürling, M., Mello, M. M., van Oosterhout, F., Domis, L. de S. and Marinho, M. M.: Response of natural cyanobacteria and algae assemblages to a nutrient pulse and elevated temperature, Front. Microbiol., 9(AUG), doi:10.3389/fmicb.2018.01851, 2018.

Madigan, M. T. and Jung, D. O.: An Overview of Purple Bacteria: Systematics, Physiology, and Habitats, in The Purple Phototrophic Bacteria. Advances in Photosynthesis and Respiration, edited by C. N. Hunter, F. Daldal, M. C. Thurnauer, and J. T. Beatty, pp. 1–15, Springer, Dordrecht., 2009.

Makri, S., Lami, A., Lods-Crozet, B. and Loizeau, J.-L.: Reconstruction of trophic state shifts over the past

665 90 years in a eutrophicated lake in western Switzerland, inferred from the sedimentary record of photosynthetic

666 pigments, J. Paleolimnol., 61(2), doi:10.1007/s10933-018-0049-5, 2019.

667 Makri, S., Rey, F., Gobet, E., Gilli, A., Tinner, W. and Grosjean, M.: Early human impact in a 15,000-year high-

668 resolution hyperspectral imaging record of paleoproduction and anoxia from a varved lake in Switzerland, Quat.

669 Sci. Rev., 239, 106335, doi:https://doi.org/10. 1016/j.quascirev.2020.106335, 2020.

670 Manske, A. K., Glaeser, J., Kuypers, M. M. M. and Overmann, J.: Physiology and Phylogeny of Green Sulfur

671 Bacteria Forming a Monospecific Phototrophic Assemblage at a Depth of 100 Meters in the Black Sea, Appl.

672 Environ. Microbiol., 71(12), 8049 LP – 8060, doi:10.1128/AEM.71.12.8049-8060.2005, 2005.

673 Mantoura, R. F. C. and Llewellyn, C. A.: The rapid determination of algal chlorophyll and carotenoid pigments

674 and their breakdown products in natural waters by reverse-phase high-performance liquid chromatography, Anal.

675 Chim. Acta, 151(Supplement C), 297–314, 1983.

676 Marcisz, K., Kołaczek, P., Gałka, M., Diaconu, A.-C. and Lamentowicz, M.: Exceptional hydrological stability

677 of a Sphagnum-dominated peatland over the late Holocene, Quat. Sci. Rev., 231, 106180,

678 doi:https://doi.org/10.1016/j.quascirev.2020.106180, 2020.

679 Meyers, P. A.: Applications of organic geochemistry to paleolimnological reconstructions: A summary of

680 examples from the Laurentian Great Lakes, in Organic Geochemistry, vol. 34, pp. 261–289, Pergamon., 2003.

681 Montesinos, E., Guerrero, R., Abella, C. and Esteve, I.: Ecology and Physiology of the Competition for Light

682 Between Chlorobium limicola and Chlorobium phaeobacteroides in Natural Habitats, Appl. Environ. Microbiol.,

683 46(5), 1007–1016, doi:10.1128/aem.46.5.1007-1016.1983, 1983.

684 Munsell Color (Firm): Munsell soil color charts : with genuine Munsell color chips, 2009 year revised. Grand

685 Rapids, MI : Munsell Color, 2010. [online] Available from:

686 https://search.library.wisc.edu/catalog/9910109259802121, 2010.

687 Murtagh, F. and Legendre, P.: Ward's Hierarchical Agglomerative Clustering Method: Which Algorithms

688 Implement Ward's Criterion?, J. Classif., 31(3), 274–295, doi:10.1007/s00357-014-9161-z, 2014.

689 Naeher, S., Smittenberg, R. H., Gilli, A., Kirilova, E. P., Lotter, A. F. and Schubert, C. J.: Impact of recent lake

690 eutrophication on microbial community changes as revealed by high resolution lipid biomarkers in Rotsee

691 (Switzerland), Org. Geochem., 49, 86–95, doi:10.1016/j.orggeochem.2012.05.014, 2012.

692 Naeher, S., Gilli, A., North, R. P., Hamann, Y. and Schubert, C. J.: Tracing bottom water oxygenation with

693 sedimentary Mn/Fe ratios in Lake Zurich, Switzerland, Chem. Geol., 352, 125–133,

694 doi:10.1016/j.chemgeo.2013.06.006, 2013.

695 Oksanen, J., Kindt, R., Pierre, L., O'Hara, B., Simpson, G. L., Solymos, P., Stevens, M. H. . H. H., Wagner, H.,

696 Blanchet, F. G., Kindt, R., Legendre, P., Minchin, P. R., O'Hara, R. B., Simpson, G. L., Solymos, P., Stevens,

697 M. H. . H. H. and Wagner, H.: vegan: Community Ecology Package, R package version 2.4-0, R Packag. version

698 2.2-1 [online] Available from: http://vegan.r-forge.r-project.org, 2016.

699 Oren, A.: 12 - Characterization of Pigments of Prokaryotes and Their Use in Taxonomy and Classification, in

700 Taxonomy of Prokaryotes, vol. 38, edited by F. Rainey and A. B. T.-M. in M. Oren, pp. 261–282, Academic

701 Press., 2011.

702 Parkin, T. B. and Brock, T. D.: Photosynthetic bacterial production in lakes: The effects of light intensity,

703 Limnol. Oceanogr., 25(4), 711–718, doi:10.4319/lo.1980.25.4.0711, 1980.

704 Pearson, F. J. and Coplen, T. B.: Stable Isotope Studies of Lakes, in Lakes, edited by A. Lerman, pp. 325–339,

705 Springer, New York, NY., 1978.

706 Poraj-Górska, A. I., Żarczyński, M. J., Ahrens, A., Enters, D., Weisbrodt, D. and Tylmann, W.: Impact of

707 historical land use changes on lacustrine sedimentation recorded in varved sediments of Lake Jaczno,

708 northeastern Poland, Catena, 153, 182–193, doi:10.1016/j.catena.2017.02.007, 2017.

709 R Core Team: R: A language and environment for statistical computing., [online] Available from: http://www.r-

710 project.org, 2015.

711 Reimer, P. J., Bard, E., Bayliss, A., Beck, J. W., Blackwell, P. G., Ramsey, C. B., Buck, C. E., Cheng, H.,

712 Edwards, R. L., Friedrich, M., Grootes, P. M., Guilderson, T. P., Haflidason, H., Hajdas, I., Hatté, C., Heaton, T.

713 J., Hoffmann, D. L., Hogg, A. G., Hughen, K. A., Kaiser, K. F., Kromer, B., Manning, S. W., Niu, M., Reimer,

714 R. W., Richards, D. A., Scott, E. M., Southon, J. R., Staff, R. A., Turney, C. S. M. and van der Plicht, J.:

715 IntCal13 and Marine13 Radiocarbon Age Calibration Curves 0–50,000 Years cal BP, Radiocarbon, 55(4), 1869–

716 1887, doi:10.2458/azu_js_rc.55.16947, 2013.

717 Sanchini, A., Szidat, S., Tylmann, W., Vogel, H., Wacnik, A. and Grosjean, M.: A Holocene high-resolution

718 record of aquatic productivity, seasonal anoxia and meromixis from varved sediments of Lake Łazduny, North-

719 Eastern Poland: insight from a novel multi-proxy approach, J. Quat. Sci., in press, 2020.

720 Schindler, D. W.: Recent advances in the understanding and management of eutrophication, Limnol. Oceanogr.,

721 51(1part2), 356–363, doi:https://doi.org/10.4319/lo.2006.51.1_part_2.0356, 2006.

722 Schneider, T., Rimer, D., Butz, C. and Grosjean, M.: A high-resolution pigment and productivity record from the

723 varved Ponte Tresa basin (Lake Lugano, Switzerland) since 1919: insight from an approach that combines

724 hyperspectral imaging and high-performance liquid chromatography, J. Paleolimnol., 60(3), 381–398,

725 doi:10.1007/s10933-018-0028-x, 2018.

726 Schnurrenberger, D., Russell, J. and Kelts, K.: Classification of lacustrine sediments based on sedimentary

727 components, J. Paleolimnol., 29(2), 141–154, doi:10.1023/A:1023270324800, 2003.

728 Smith, V. H. and Schindler, D. W.: Eutrophication science: where do we go from here?, Trends Ecol. Evol.,

729 24(4), 201–207, doi:https://doi.org/10.1016/j.tree.2008.11.009, 2009.

730 Smol, J. P.: The power of the past: using sediments to track the effects of multiple stressors on lake ecosystems,

731 Freshw. Biol., 55(Suppl. 1), 43–59, doi:doi:10.1111/j.1365-2427.2009.02373.x, 2010.

732 Stuiver, M. and Reimer, P. J.: Extended 14C data base and revised CALIB 3.0 14C age calibration program,

733 Radiocarbon, 35(1), 215–230, doi:10.1017/S0033822200013904, 1993.

734 Szidat, S., Salazar, G. A., Vogel, E., Battaglia, M., Wacker, L., Synal, H.-A. and Türler, A.: 14C Analysis and

735 Sample Preparation at the New Bern Laboratory for the Analysis of Radiocarbon with AMS (LARA),

736 Radiocarbon, 56(02), 561–566, doi:10.1017/s0033822200049602, 2014.

737 Tõnno, I., Nauts, K., Belle, S., Nõmm, M., Freiberg, R., Kõiv, T. and Alliksaar, T.: Holocene shifts in the

738 primary producer community of large, shallow European Lake Peipsi, inferred from sediment pigment analysis,

739 J. Paleolimnol., 61(4), 403–417, doi:10.1007/s10933-019-00067-3, 2019.

740 Tu, L., Jarosch, K. A., Schneider, T. and Grosjean, M.: Phosphorus fractions in sediments and their relevance for

741 historical lake eutrophication in the Ponte Tresa basin (Lake Lugano, Switzerland) since 1959, Sci. Total

742 Environ., 685, 806–817, doi:10.1016/j.scitotenv.2019.06.243, 2019.

743 Tylmann, W., Zolitschka, B., Enters, D. and Ohlendorf, C.: Laminated lake sediments in northeast Poland:

744 Distribution, preconditions for formation and potential for paleoenvironmental investigation, J. Paleolimnol.,

745 50(4), 487–503, doi:10.1007/s10933-013-9741-7, 2013.

746 Vitousek, P. M., Cassman, K., Cleveland, C., Crews, T., Field, C. B., Grimm, N. B., Howarth, R. W., Marino,

747 R., Martinelli, L., Rastetter, E. B. and Sprent, J. I.: Towards an ecological understanding of biological nitrogen

748 fixation, in Biogeochemistry, vol. 57–58, pp. 1–45., 2002.

749 Weisbrodt, D., Enters, D., Żarczyński, M. J., Poraj-Górska, A. I. and Tylmann, W.: Contribution of non-pollen

750 palynomorphs to reconstructions of land-use changes and lake eutrophication: case study from Lake Jaczno,

751 northeastern Poland, Limnol. Rev., 16(4), 247–256, doi:10.1515/limre-2016-0027, 2017.

752 Wetzel, R. G.: Limnology: Lake and River Ecosystems, 3rd ed., Acedemic Press., 2001.

753 Wirth, S. B., Gilli, A., Niemann, H., Dahl, T. W., Ravasi, D., Sax, N., Hamann, Y., Peduzzi, R., Peduzzi, S.,

754 Tonolla, M., Lehmann, M. F. and Anselmetti, F. S.: Combining sedimentological, trace metal (Mn, Mo) and

755 molecular evidence for reconstructing past water-column redox conditions: The example of meromictic Lake

756 Cadagno (Swiss Alps), Geochim. Cosmochim. Acta, 120, 220–238, doi:10.1016/j.gca.2013.06.017, 2013.

757 Woolway, R. I. and Merchant, C. J.: Worldwide alteration of lake mixing regimes in response to climate change,

758 Nat. Geosci., 12(4), 271–276, doi:10.1038/s41561-019-0322-x, 2019.

759 Yurkov, V. V and Beatty, J. T.: Aerobic Anoxygenic Phototrophic Bacteria, Microbiol. Mol. Biol. Rev., 62(3),

760 695 LP – 724 [online] Available from: http://mmbr.asm.org/content/62/3/695.abstract, 1998.

761 Zander, P. D., Szidat, S., Kaufman, D. S., Żarczyński, M., Poraj-górska, A. I. and Grosjean, M.: Miniature

762 radiocarbon measurements (< 150 μg C) from sediments of Lake Żabińskie , Poland : effect of precision and

763 dating density on age- depth models, Geochronology, 2(April), 63–79, doi:10.5194/gchron-2-63-2020, 2020.

764 Zolitschka, B., Francus, P., Ojala, A. E. K. and Schimmelmann, A.: Varves in lake sediments - a review, Quat.

765 Sci. Rev., 117, 1–41, doi:10.1016/j.quascirev.2015.03.019, 2015.

766 Züllig, H.: Untersuchungen über die Stratigraphie von Carotinoiden im geschichteten Sediment von 10

767 Schweizer Seen zur Erkundung früherer Phytoplankton-Entfaltungen, Schweizerische Zeitschrift für Hydrol.,

768 44(1), 1–98, 1982.

769 Züllig, H.: Role of carotenoids in lake sediments for reconstructing trophic history during the late Quaternary, J.

770 Paleolimnol., 2(1), 23–40, doi:10.1007/BF00156982, 1989.

771

772

773

774

775

776

777

778

779

780

781

782
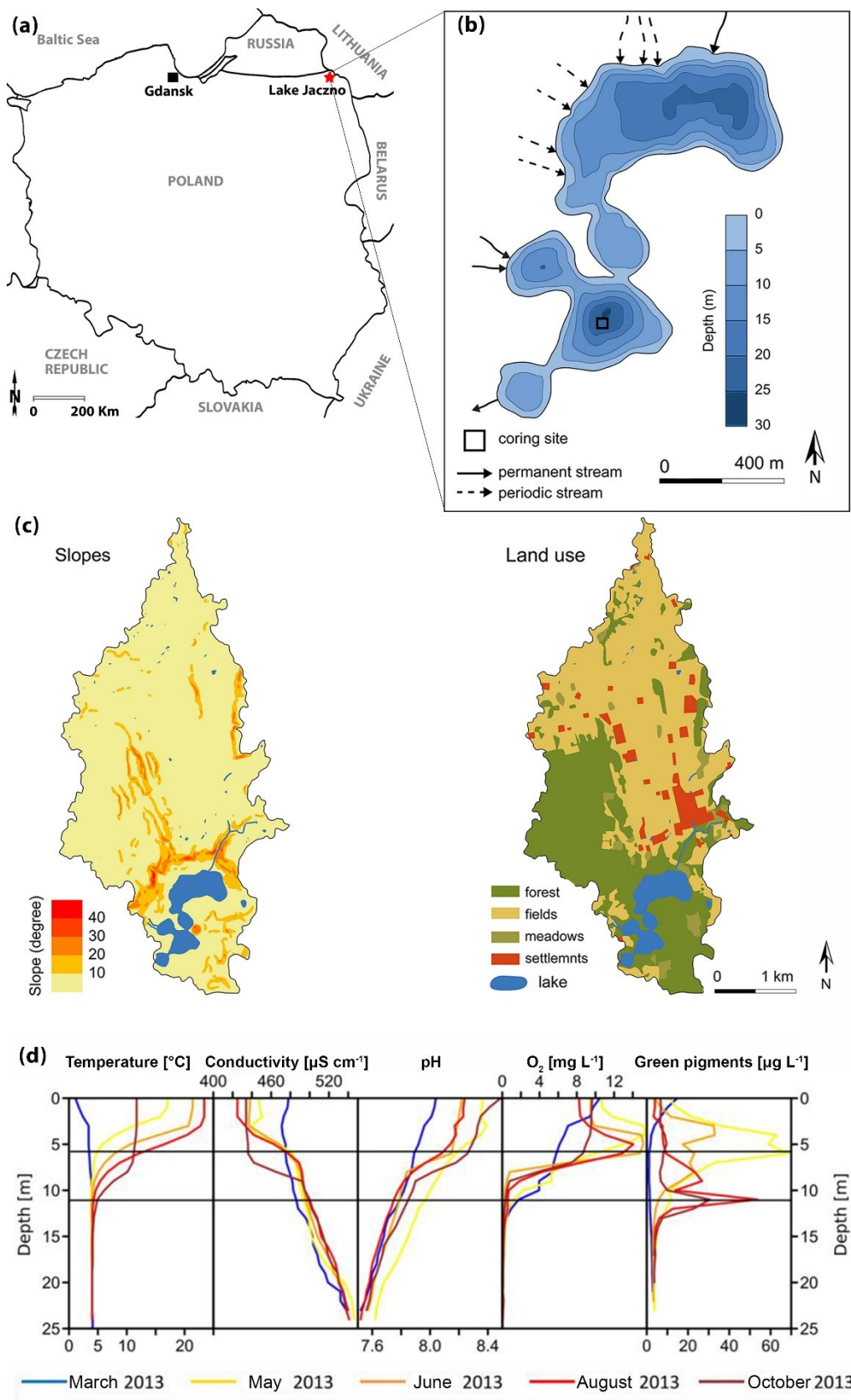
Figure 1: a) Localization of Lake Jaczno. b) Lake bathymetry (modified from Poraj-Górska et al., 2017) and coring position c) Slopes and land use maps of the catchment (modified from Poraj-Górska et al., 2017) d) Seasonal limnological parameters in 2013 CE (Butz et al., 2016).

786
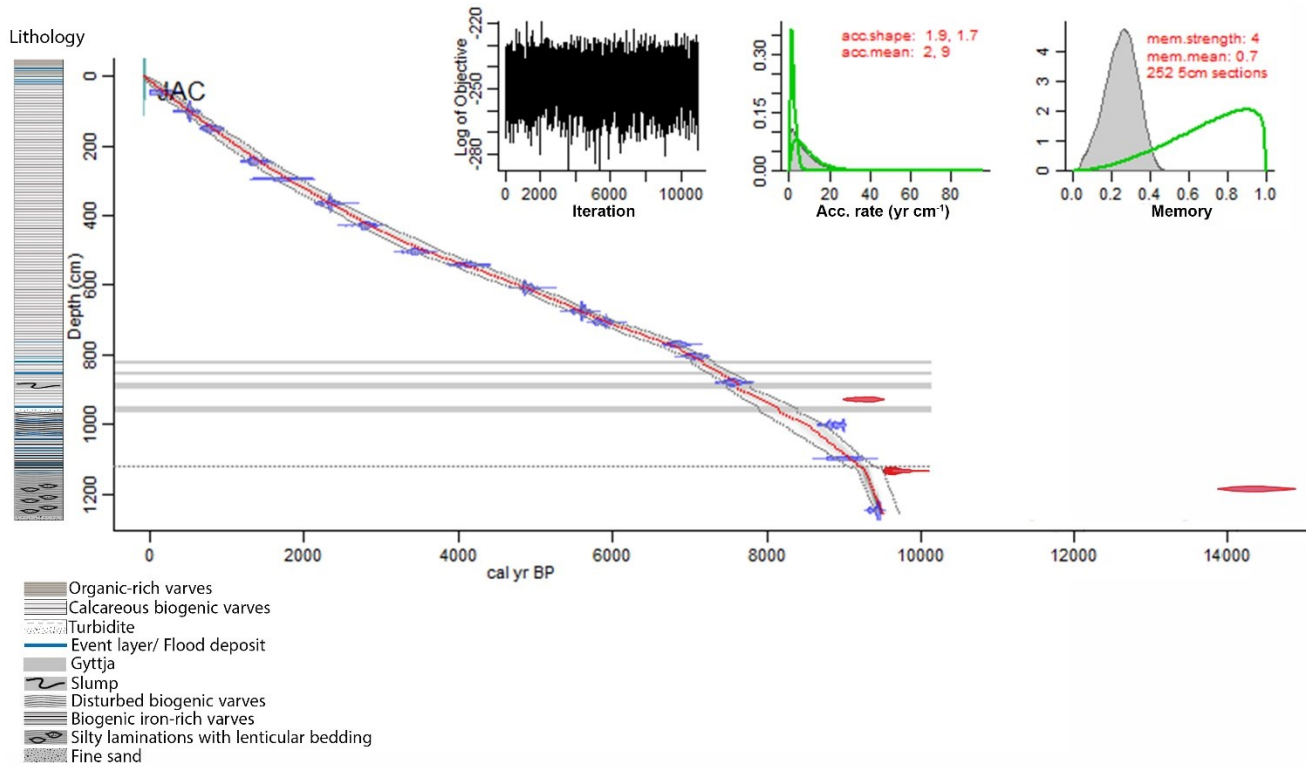
Figure 2: Age depth model and lithology of Lake Jaczno. The red line is the modelled chronology using Bacon (Blaauw and Christeny, 2011; Blaauw et al., 2020); the excluded outliers are shown in red. The grey dotted lines indicate the 95 % (2σ) probabilities. The grey horizontal areas indicate event layers (>3 cm) excluded from the model. The horizontal dashed line marks the boundary of a higher sedimentation rate (model parameter). The upper left panel shows the log objective vs. MCMC iteration that indicates a stationary distribution. The middle and right panels indicate the distributions (prior in green, posterior in grey) for the accumulation rate and the memory, respectively.

807

808
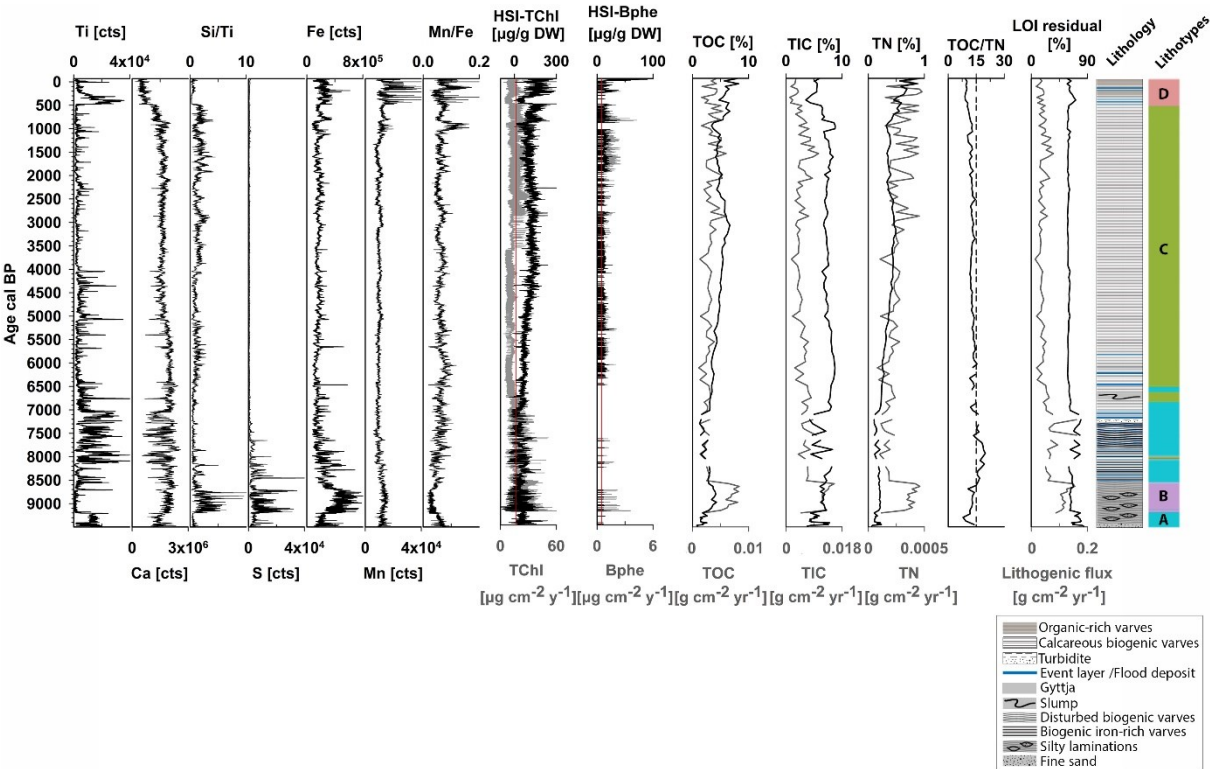
809 **Figure 3: Selected biogeochemical proxies that defined the four sedimentary lithotypes A–D (in different**

810 **color) after unconstrained clustering and PCA analysis (Fig. S2). On the right: sediment lithology based on**

811 **visual examination.**

812

813

814

815

816

817

818

819

820

821

822

823

824

825
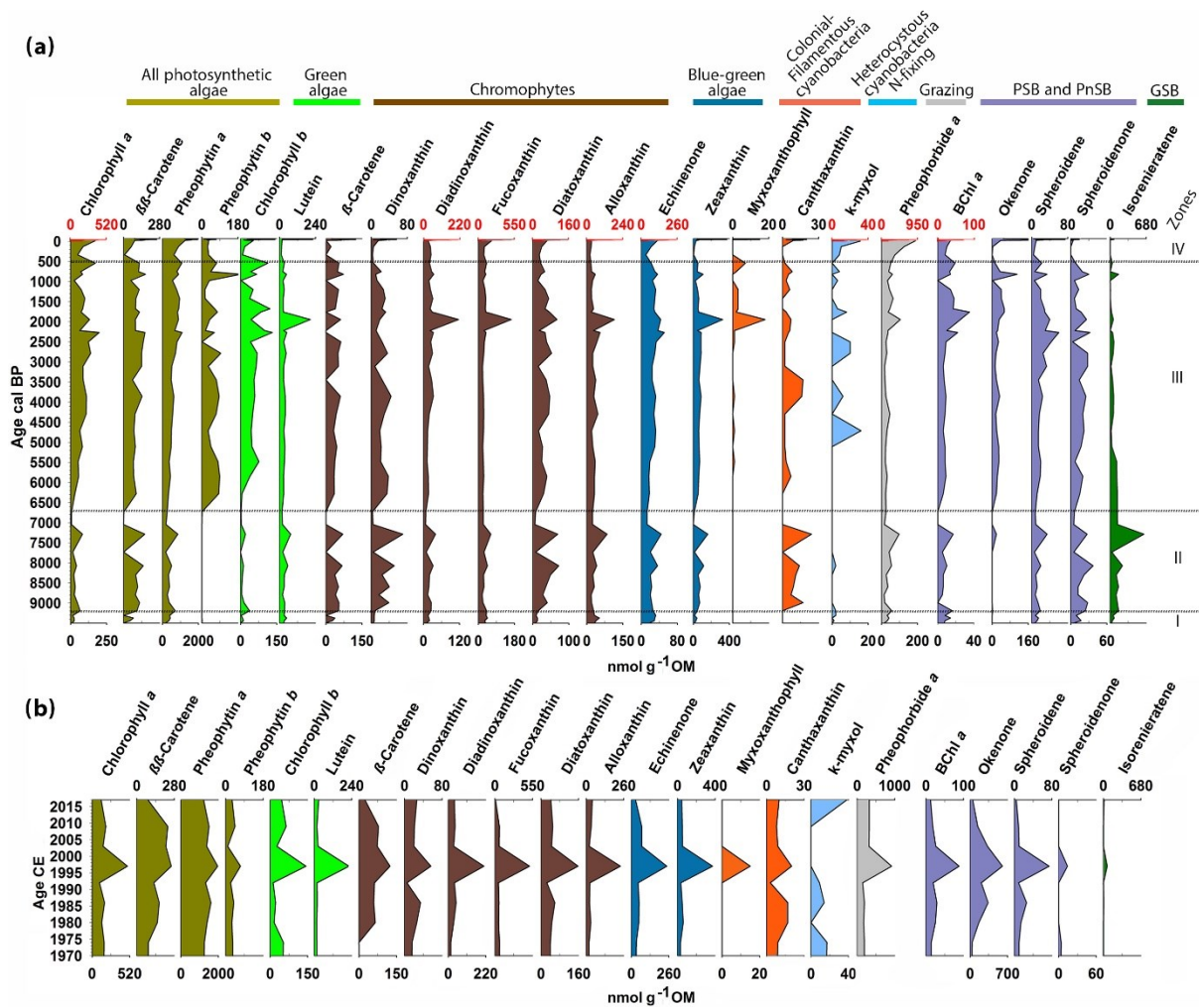
Figure 4: Chlorophyll, chlorophyll derivatives, carotenoids and bacterial pigments concentrations measured by HPLC a) for the entire Holocene, and b) for the last 50 years. The zones are defined by constrained hierarchical clustering. The different colors indicate different algal groups based on the pigments' taxa affiliation. The occasional red scale on top marks the significantly higher concentrations of these pigments in the last 50 years.

839
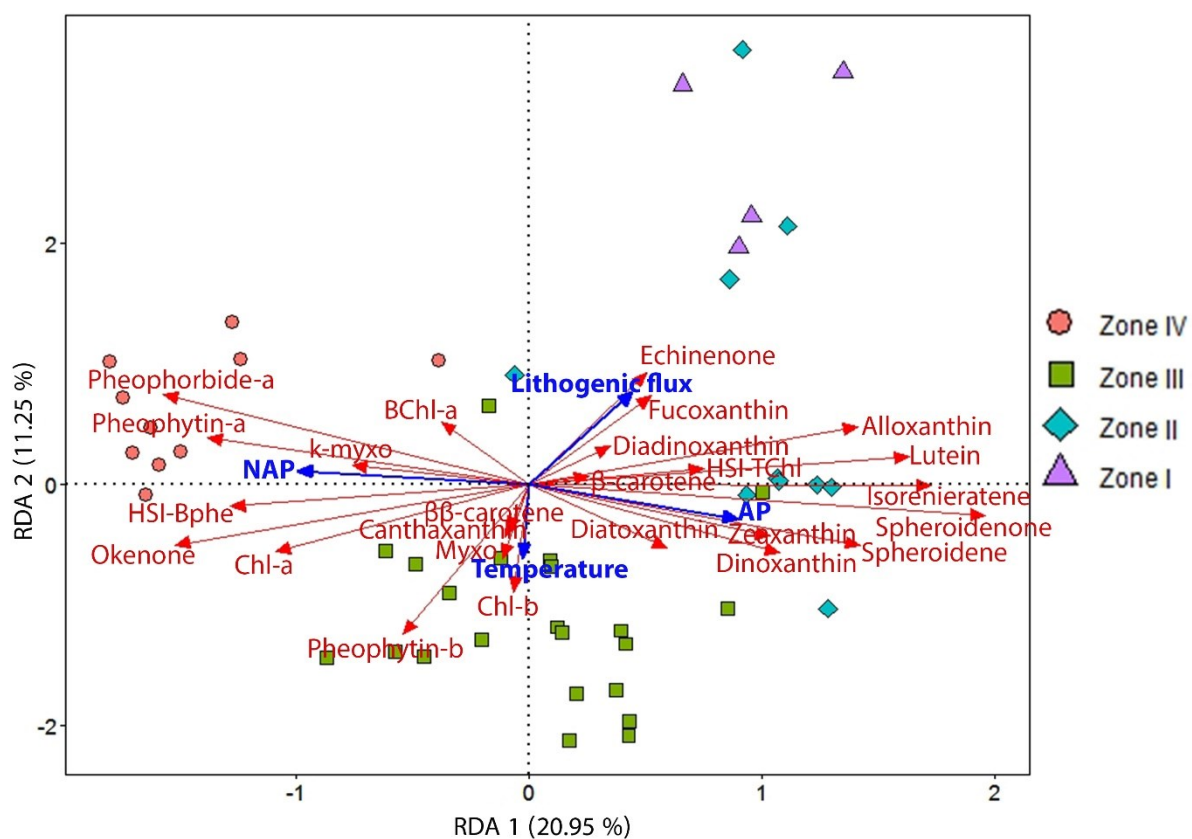
840 **Fig 5: RDA triplot showing the explanatory variables (AP, NAP, temperature and lithogenic flux) in blue,**

841 **and the response variables (HPLC- and HSI-inferred pigment concentrations) in red. The samples are**

842 **grouped according to the pigment zones (Fig. 4a).**

843

844
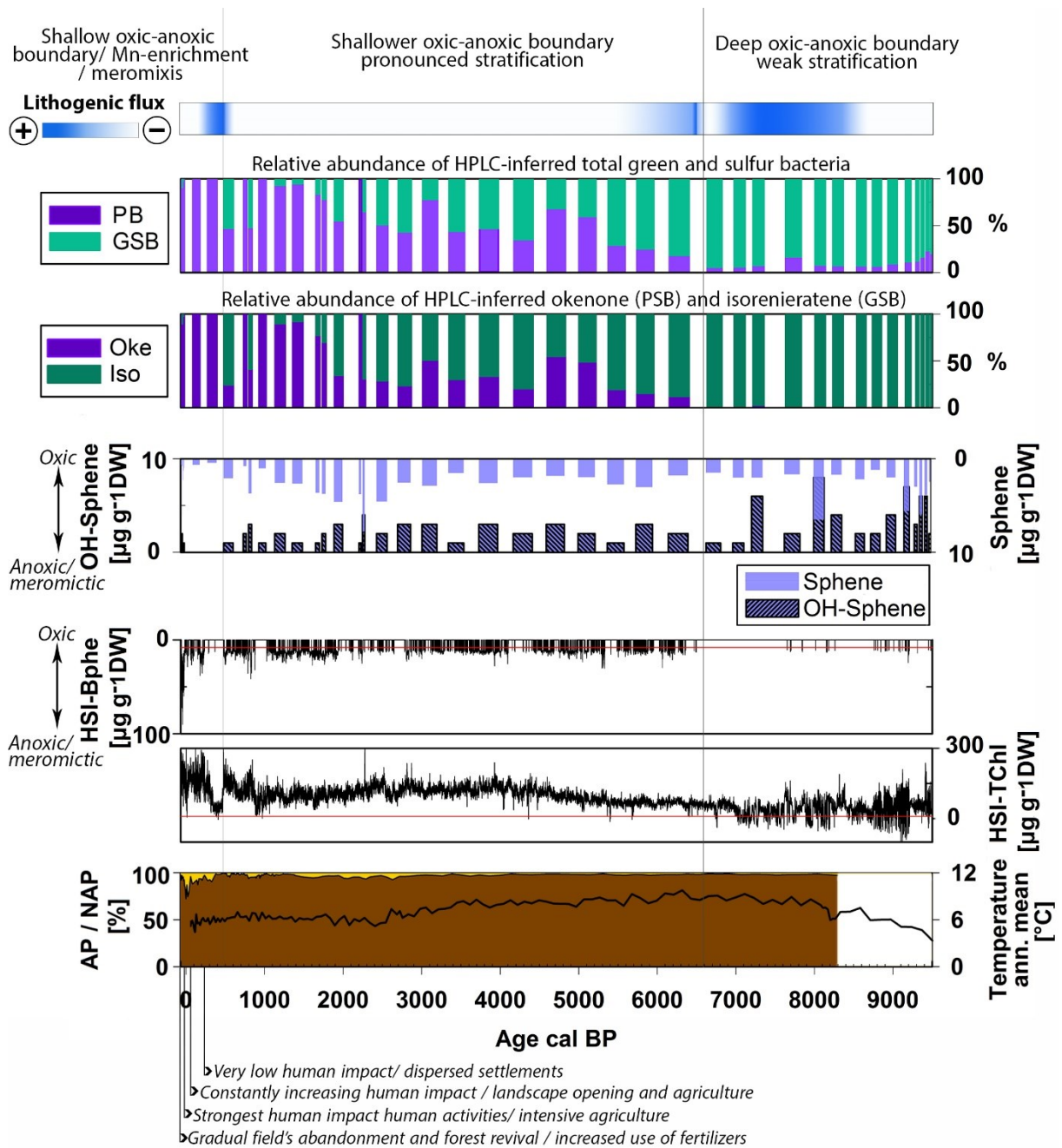
Figure 6: Holocene summary of the relative abundance of purple bacteria (sum of PSB and PnSB) and GSB, *Chromatium* **(okenone, PSB) and** *Clorobium* **(isorenieratene, GSB), the content of spheroidene and spheroidenone pigments produced by** *R. sphaeroides* **(PnSB), and the high-resolution calibrated HSI-TChl and HSI-Bphe concentrations. Top: indication of lithogenic flux and general evolution of the chemocline. Bottom: AP/NAP percentages (Kinder et al., 2019; Marcisz et al., 2020) with archaeological evidence of human impact, and the annual mean temperature variability (Heikkilä and Seppä, 2010).**

851

852

853

Table 1: Radiocarbon age results and calibrated ages. Uncertainties for ^{14}C ages refer to 68 % probabilities (1σ), whereas ranges of calibrated ages refer to 95 % probabilities (2σ). Outlier samples are marked with an asterisk. Indet: indeterminable, dicot: dicotyledonous.

Sample ID	Material	C mass (µg C)	Age ^{14}C BP	Age (cal BP)[a]	Age range (cal BP)[b]	Graphite /Gas
BE-10957.1.1	*Betula alba* fruit, woody scale, *Pinus sylvestris* needle base	104	132±64	142	0–284	gas
BE-10958.1.1	*Betula alba* fruit scale, woody scale, dicot leaf fragment	219	482±44	755	679–904	graphite
BE-10959.1.1	*Pinus sp.* periderm, coniferous wood and periderm fragment, *Betula alba* fruit fragments, coniferous scales	118	872±55	790	694–912	graphite
BE-10960.1.1	*Pinus sp.* periderm, *Betula alba* fruit fragments, conifer scale, Pinus sp. periderm, *Betula alba* fruit fragments	64	1460±67	1364	1283–1522	gas
BE-10961.1.1	*Betula alba* fruit fragments, conifer scale, *Betula alba* fruit, semi–charred periderm	19	1781±127	1706	1410–1987	gas
BE-10962.1.1	*Alnus glutinosa* fruit, *Betula alba* fruit fragments, needle/leaf indet, male anthere indet	268	2321±39	2341	2180–2458	graphite
BE-10963.1.1	*Betula alba* fruit fragments, *Pinus sp.* periderm, male anthere indet, *Betula alba* fruit fragments, *Pinus sp.* periderm, conifer scales	73	2677±69	2801	2545–2959	gas
BE-10964.1.1	*Betula alba* fruit fragments, *Pinus sp.* periderm, male anthere indet, *Betula alba* fruit fragments	74	3229±72	3458	3259–3633	gas
BE-10965.1.1	*Alnus glutinosa* fruit fragment, *Betula alba* fruit fragments, conifer scales, dicot leaf fragments	130	3758±60	4125	3927–4383	graphite
BE-10966.1.1	Male anthere indet, dicot leaf fragments, conifer scales, indet scale, wood indet	399	4322±36	4887	4836–4972	graphite
BE-10967.1.1	Dicot leaf fragments, indet scale, male anthere indet	428	4860±37	5601	5491–5650	graphite
BE-10968.1.1	Dicot leaf fragments, wood remains	348	5144±39	5906	5753–5989	graphite
BE-10969.1.1	Dicot leaf fragments, indet periderm, wood remains	183	5998±57	6839	6678–6977	graphite

BE-10970.1.1	Deciduous woody scale	365	6153±41	7062	6942–7166	graphite
BE-10971.1.1	*Betula alba* fruit fragments, *Pinus sp.* periderm, conifer scale, wood indet	111	6699±79	7567	7439–7674	graphite
*BE-10972.1.1	*Pinus sylvestris* needle fragments, wood indet	58	8291±99	9279	9029–9475	gas
BE-10973.1.1	Dicot leaf fragments, deciduous periderm, wood indet	996	8018±22	8896	8778–9007	graphite
BE-10974.1.1	Betula alba fruit fragments, *Pinus sylvestris* needle fragments, dicot leaf fragments	117	8094±91	9019	8651–9287	gas
*BE-10975.1.1	*Pinus sylvestris* needle fragments, *Betula alba* fruit fragments, indet periderm	280	8715±54	9677	9548–9887	graphite
*BE-10976.1.1	Dicot. leaf fragments, male anthere indet, conifer needle tip, indet periderm	308	12446±69	14580	14198–14994	graphite
BE-10977.1.1	Dicot leaf fragments, *Pinus sp.* periderm, woody scale	999	8388±22	9440	9318–9479	graphite

857   [a] Median probability (Stuiver and Reimer, 1993)

858   [b] Calibrated age range with the IntCal 13 calibration curve (Stuiver and Reimer, 1993; Reimer et al.,

859   2013)

860

861